

Gaussian process test for high-throughput sequencing time series: application to experimental evolution

Hande Topa^{1,*}, Ágnes Jónás^{2,3*}, Robert Kofler²,
Carolin Kosiol² and Antti Honkela⁴

¹ Helsinki Institute for Information Technology HIIT, Department of
Information and Computer Science, Aalto University, Espoo, Finland

² Institut für Populationsgenetik, Vetmeduni Vienna, 1210 Wien, Austria

³ Vienna Graduate School of Population Genetics, Wien, Austria

⁴ Helsinki Institute for Information Technology HIIT, Department of
Computer Science, University of Helsinki, Helsinki, Finland

Abstract

Motivation: Recent advances in high-throughput sequencing (HTS) have made it possible to monitor genomes in great detail. New experiments not only use HTS to measure genomic features at one time point but to monitor them changing over time with the aim of identifying significant changes in their abundance. In population genetics, for example, allele frequencies are monitored over time to detect significant frequency changes that indicate selection pressures. Previous attempts at analysing data from HTS experiments have been limited as they could not simultaneously include data at intermediate time points, replicate experiments and sources of uncertainty specific to HTS such as sequencing depth.

Results: We present the beta-binomial Gaussian process (BBGP) model for ranking features with significant non-random variation in abundance over time. The features are assumed to represent proportions, such as proportion of an alternative allele in a population. We use the beta-binomial model to capture the uncertainty arising from finite sequencing depth and combine it with a Gaussian process model over the time series. In simulations that mimic the features of experimental evolution data, the proposed method clearly outperforms classical testing in average precision of finding selected alleles. We also present simulations exploring different experimental design choices and results on real data from *Drosophila* experimental evolution experiment in temperature adaptation.

Availability: R software implementing the test is available at <https://github.com/handetopa/BBGP>.

1 Introduction

Most biological processes are dynamic and analysis of time series data is necessary to understand them. Recent advances in high-throughput sequencing (HTS) technologies have provided new experimental approaches to collect genome-wide time series. For example, experimental evolution now uses a new evolve and re-sequencing (ER) approach to understand which genes are

*The authors wish it to be known that in their opinion, the first two authors should be regarded as joint first authors.

targeted by selection and how (Burke and Long, 2012, Kawecki *et al.*, 2012). Such experiments enable phenotypic divergence to be forced in response to changes in only few environmental conditions in the laboratory while other conditions are kept constant. The evolved populations are then subjected to HTS.

Experimental evolution in microorganisms has focused on the fate new mutations. For example, in *Escherichia coli* (Barrick *et al.*, 2009) and *Saccharomyces cerevisiae* (Lang *et al.*, 2013) new mutations were studied. In contrast, ER experiments with sexually reproducing multicellular organisms address selection on standing variation and allele frequency changes (AFCs) in small populations where drift plays an important role. For example, for *Drosophila melanogaster* (*Dmel*), several phenotypic traits, such as accelerated development (Burke *et al.*, 2010), body size variation (Turner *et al.*, 2011), hypoxia-tolerance (Zhou *et al.*, 2011) and temperature adaptation (Orozco-Ter Wengel *et al.*, 2012) have been investigated. Motivated by these experimental studies, we believe that experimental evolution combined with HTS supplies a good basis for studying AFC through time series molecular data.

To perform allele frequency comparisons, pairwise statistical tests between base and evolved populations were typically carried out. Burke *et al.* (2010) combined Fisher’s exact tests with a sliding-window approach to identify genomic regions that show allele frequency differences between populations selected for accelerated development and controls without direct selection. Turner *et al.* (2011) developed a pairwise summary statistic, called ”diff-Stat” to estimate the observed distribution of allele frequency differences and compared this to the expected distribution without selection. Orozco-Ter Wengel *et al.* (2012) identify SNPs with a consistent AFC among replicates by performing a Cochran-Mantel-Haenszel test (CMH) (Agresti, 2002). The latter is an extension of the Fisher’s exact test to multiple replicates. All above-mentioned statistical methods are based on pairwise comparisons between the base and evolved populations and they do not take full advantage of the time series data now available. Bollback *et al.* (2008) developed a method to analyse time series data based on population genetic models and estimated the effective population size N_e of a bacteriophage from a single locus. Illingworth *et al.* (2012) derived a model for time series data from large populations of microorganisms ($N_e \approx 10^8$) where drift can be ignored and the population allele frequencies evolve ”quasi-deterministically”. Here, we propose an alternative Gaussian process (GP) based approach to study AFCs over the entire time series experiment genome-wide for small populations ($N_e \approx 10^2 - 10^3$).

GP is a non-parametric statistical model that is extremely well-suited for modelling HTS time series data which usually have relatively few time points that may be irregularly sampled. Recently, there have been some works applying GP models with parameters describing the process of evolution (e.g., Jones and Moriarty, 2013 account for phylogenetic relationships, Palacios and Minin, 2013 for effective population size). GPs have also recently been applied to gene expression time series by a number of authors (Yuan, 2006; Gao *et al.*, 2008; Kirk and Stumpf, 2009; Liu *et al.*, 2010; Honkela *et al.*, 2010; Stegle *et al.*, 2010; Cooke *et al.*, 2011; Kalaitzis and Lawrence, 2011; Titsias *et al.*, 2012; Liu and Niranjana, 2012; Äijö *et al.*, 2013; Hensman *et al.*, 2013). In differential analysis, GPs have been applied to detect differences in gene expression time series in a two-sample setting by Stegle *et al.* (2010) and for detecting significant changes by Kalaitzis and Lawrence (2011). While these methods provide a very sensible basis for detecting the changing alleles, they fail to properly take into account all aspects of the available HTS data, such as differences in sequencing depth between different alleles and time points. These differences can have a huge impact in the reliability of different measured allele frequencies and taking them into account is vital for achieving good accuracy with the available short time series.

2 Methods

To identify the candidate alleles which evolve under selection, we model the allele frequencies by Gaussian Process (GP) regression. We fit time-dependent and time-independent GP models and rank the alleles according to their corresponding Bayes factors, i.e. the ratio of the marginal likelihoods under the different models.

GPs provide a convenient approach for modelling short time series. However, when applying them to a large number of short parallel time series as in many genomic applications, naive application leads to overfitting or underfitting in some examples. While these problems are rare, the bad examples can easily dominate the ranking. We overcome these challenges by excluding nonsensical parameter values, for example using a good variance model that can be incorporated into the GP models.

2.1 Data and Preprocessing

In the following, we use the term SNP for the markers and alleles under study, but the methods can be applied to any features whose abundance can be quantified in a similar manner. We consider SNPs that are bi-allelic for a specific position of the genome in a population. Multi-allelic SNPs, however, exist but are rare and likely to be sequencing errors (Burke *et al.*, 2010). Multi-allelic cases can be treated by simply ignoring the least frequent allele or transformed to bi-allelic site by summing up the frequencies of the most infrequent alleles. Here, we assumed that only two of the alleles from (A, T, C, G) can be observed at each SNP position. We first determine the abundances of these two specific alleles and we aim to model the time dependency of the rising allele’s frequency over several generations. We will refer to generations as time points for simplicity.

We denote the replicate index of each observation by r_j and the time point by t_j , $j = 1, \dots, J$, with J denoting the total number of observations. For each of these points, we assume HTS reads have been aligned to a reference genome with y_{ij} reads with a specific allele at SNP position i . We use n_{ij} to denote the total sequencing depth at the position.

2.2 Mean and Variance Inference: Beta-Binomial Model

We model y_{ij} as a draw from a binomial distribution with parameters n_{ij} and p_{ij} :

$$y_{ij}|n_{ij}, p_{ij} \sim \text{Bin}(n_{ij}, p_{ij}), \quad (1)$$

where p_{ij} denotes the frequency of the specific allele in the population. We set a uniform Beta(1,1) prior on p_{ij} :

$$p_{ij}|\alpha, \beta \sim \text{Beta}(\alpha, \beta), \quad (2)$$

where $\alpha = 1$, $\beta = 1$.

Since beta prior is conjugate to the binomial likelihood, the posterior distribution will also be a beta distribution:

$$p_{ij}|y_{ij}, n_{ij}, \alpha, \beta \sim \text{Beta}(\alpha_{ij}^*, \beta_{ij}^*), \quad (3)$$

where

$$\begin{aligned} \alpha_{ij}^* &= \alpha + y_{ij}, \\ \beta_{ij}^* &= \beta + n_{ij} - y_{ij}. \end{aligned}$$

Then, the posterior mean and variance of p_{ij} can be calculated as:

$$E(p_{ij}|y_{ij}, n_{ij}, \alpha, \beta) = \frac{\alpha_{ij}^*}{\alpha_{ij}^* + \beta_{ij}^*} = \frac{\alpha + y_{ij}}{\alpha + \beta + n_{ij}} \quad (4)$$

$$\begin{aligned} \text{Var}(p_{ij}|y_{ij}, n_{ij}, \alpha, \beta) &= \frac{\alpha_{ij}^* \beta_{ij}^*}{(\alpha_{ij}^* + \beta_{ij}^*)^2 (\alpha_{ij}^* + \beta_{ij}^* + 1)} \\ &= \frac{(\alpha + y_{ij})(\beta + n_{ij} - y_{ij})}{(\alpha + \beta + n_{ij})^2 (\alpha + \beta + n_{ij} + 1)}. \end{aligned} \quad (5)$$

The inferred posterior means and posterior variances are used to fit the GP models as described in the following sections. As the results will show, this step is very important for incorporating the available uncertainty information into the GP models by taking into account different sequencing depths. For example, beta-binomial model assigns larger variances to the alleles with lower sequencing depths (Fig. 1). Moreover, the Beta(1,1) prior on p_{ij} leads to a symmetry in the posterior mean and variance. Therefore, the result of our method is not affected whichever allele is chosen from the alternative alleles.

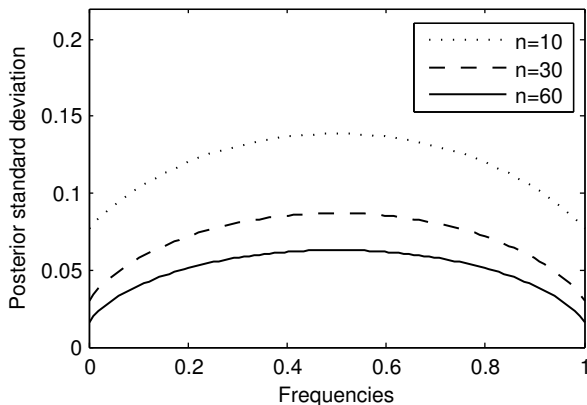


Figure 1: Posterior standard deviations of the allele frequencies with sequencing depths 10, 30, and 60.

2.3 Gaussian Process Regression

A **Gaussian process (GP)** is a collection of random variables, any finite number of which have a joint Gaussian distribution. We write

$$f(t) \sim \mathcal{GP}(m(t), K(t, t')) \quad (6)$$

to denote that $f(t)$ follows a Gaussian process with mean function $m(t) = E[f(t)]$ and covariance function $K(t, t') = E[(f(t) - m(t))(f(t') - m(t'))]$. We let $\mathbf{y} = (y_i)_{i=1}^N$ be a vector of the noisy observations measured at points $\mathbf{t} = (t_i)_{i=1}^N$ satisfying

$$y_i = f(t_i) + \epsilon, \quad (7)$$

where ϵ is Gaussian observation noise with zero mean and a diagonal covariance matrix Σ_ϵ . To simplify the algebra we assume the mean function $m(t) = 0$ and subtract the mean of \mathbf{y} .

Gaussian processes allow marginalising the latent function to obtain a marginal likelihood. The covariance function K and the noise covariance Σ_ϵ depend on hyperparameters and parameters θ that can be estimated by maximising the log marginal likelihood:

$$\log(p(\mathbf{y}|\mathbf{t}, \theta)) = -\frac{1}{2}\mathbf{y}^T[K(\mathbf{t}, \mathbf{t}) + \Sigma_\epsilon]^{-1}\mathbf{y} - \frac{1}{2}\log|K(\mathbf{t}, \mathbf{t}) + \Sigma_\epsilon| - \frac{N}{2}\log(2\pi), \quad (8)$$

where $K(\mathbf{t}, \mathbf{t})$ denotes the covariance matrix constructed by evaluating the covariance function at points \mathbf{t} . It is also possible to compute the posterior mean and covariance at non-sampled time points \mathbf{t}_* , given the noisy observations \mathbf{y} at sampled time points \mathbf{t} . This is often useful for visualisation purposes. We obtain (Rasmussen and Williams, 2006):

$$f_*|\mathbf{y} \sim N(m_*, \Sigma_*), \quad (9)$$

where

$$\begin{aligned} m_* &= E[f_*|\mathbf{y}] = K(\mathbf{t}_*, \mathbf{t})[K(\mathbf{t}, \mathbf{t}) + \Sigma_\epsilon]^{-1}\mathbf{y}, \\ \Sigma_* &= K(\mathbf{t}_*, \mathbf{t}_*) - K(\mathbf{t}_*, \mathbf{t})[K(\mathbf{t}, \mathbf{t}) + \Sigma_\epsilon]^{-1}K(\mathbf{t}, \mathbf{t}_*). \end{aligned}$$

In our GP models we use the squared exponential covariance matrix to model the underlying smooth function. The squared exponential covariance

$$K_{SE}(t, t') = \sigma_f^2 e^{-\frac{(t-t')^2}{2l^2}} \quad (10)$$

has two parameters: the length scale, l , and the signal variance, σ_f^2 . Length scale specifies the distance beyond which any two inputs become uncorrelated. A small length scale means that the function fluctuates very quickly, whereas a large length scale means that the function behaves like a constant function. Three example realisations generated with squared exponential covariance matrix can be seen in Fig. 2 (a).

In the standard GP model the observation noise is assumed to be white: the noise at different time points is independent and identically distributed. The corresponding covariance matrix

$$\Sigma_\epsilon = \Sigma_W = \sigma_n^2 I \quad (11)$$

is an identity matrix multiplied by the noise variance parameter, σ_n^2 . Three example realisations generated with white noise covariance matrix can be seen in Fig. 2 (b).

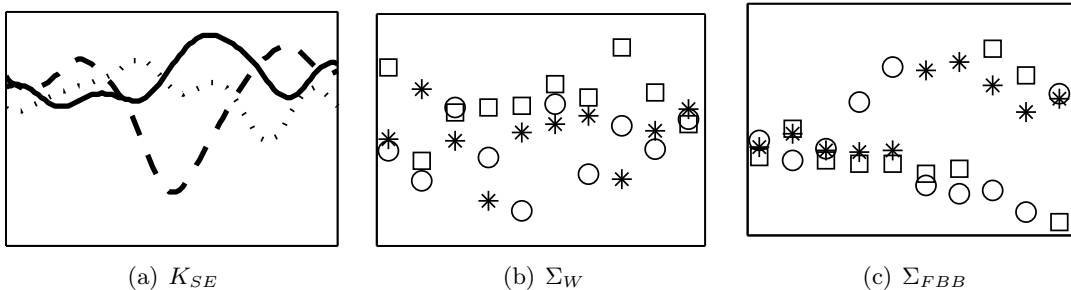


Figure 2: Example realisations from GPs and noise processes with different covariance structures.

2.4 BBGP: Beta-Binomial Gaussian Process

The Beta-Binomial Gaussian Process (BBGP) method combines beta-binomial model with the GP model in the sense that the posterior means and posterior variances of the frequencies, which are inferred by beta-binomial model, are used to fit the GP model using an additional noise covariance matrix which we call fixed beta-binomial (FBB) covariance matrix.

Returning to Sec. 2.2, let us denote the posterior mean and variance of p_{ij} by m_{ij} and s_{ij}^2 , respectively. That is,

$$m_{ij} = \mathbb{E}(p_{ij}|y_{ij}, n_{ij}, \alpha, \beta) \quad (12)$$

$$s_{ij}^2 = \text{Var}(p_{ij}|y_{ij}, n_{ij}, \alpha, \beta). \quad (13)$$

To fit the BBGP model, we assume

$$m_{ij} = f_i(t_j) + \mu_{m_i} + \epsilon, \quad (14)$$

where $f_i(t) \sim \mathcal{GP}(0, K_{SE}(t, t'))$ and $\epsilon \sim N(0, \Sigma_W + \Sigma_{FBB})$. The mean μ_{m_i} is eliminated by subtracting the mean from m_{ij} . Because of Σ_{FBB} this is an approximation that may fail if n_{ij} vary significantly, but it speeds up inference significantly. The additional covariance

$$\Sigma_{FBB} = \text{diag}(s_{ij}^2) \quad (15)$$

is a diagonal fixed beta-binomial (FBB) covariance matrix which is used to include known variance information for each observation in the GP model. The elements of Σ_{FBB} are determined by the frequency variance vector which is inferred from beta-binomial model in Sec. 2.2. Three example realisations generated with fixed beta-binomial covariance matrix can be seen in Fig. 2 (c), where larger variance values were inferred for the later time points.

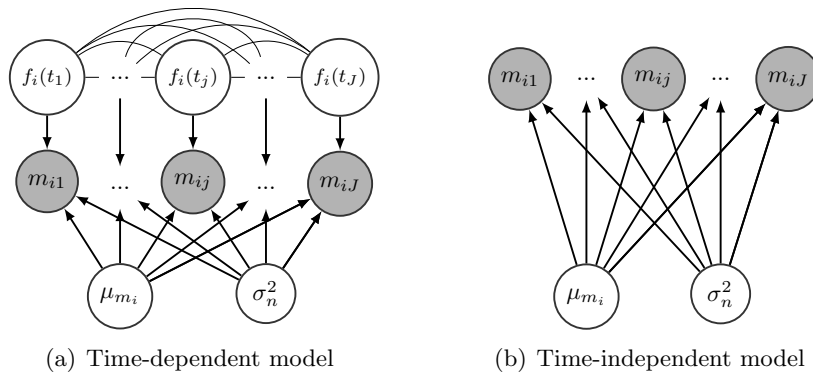


Figure 3: Graphical models for the (a) time-dependent and (b) time-independent BBGP models.

2.5 BBGP-based test

We fit the “time-dependent” BBGP model of Eq. (14) and a “time-independent” model without the GP term $f_i(t_j)$ for each SNP i . As can be seen from the graphical models in Fig. 3, “time-independent” model assumes that the observations are randomly generated around a constant mean with no temporal dependency, whereas “time-dependent” model captures the dependency between the observations by the function $f_i(t)$, which follows a GP with the squared exponential covariance function. Thereby the parameters of the squared exponential covariance (K_{SE} ,

Eq. 10) in the time-dependent model and the white noise covariance (Σ_W , Eq. 11) in both models are fitted by maximising the marginal likelihood. The fixed beta-binomial covariance (Σ_{FBB} , Eq. 15) does not contain any free hyperparameters. If the model is actually time-independent, the length scale in the squared exponential covariance is estimated to be very large, which makes the maximum likelihood of the time-dependent model equivalent to that of time-independent model. Fig. 4 shows an example of the time-dependent (left) and time-independent (right) BBGP models.

We maximise the log marginal likelihood functions for the models by scaled conjugate gradient method using the “gptk” R package by Kalaitzis and Lawrence (2011). We use a grid search over the parameter space and initialise the parameters to the grid value with highest likelihood. We also set a lower bound equal to the shortest spacing between observations for the length scale parameter to avoid overfitting.

We compute the Bayes factor (BF) for SNP i as (Stegle *et al.*, 2010; Kalaitzis and Lawrence, 2011):

$$\text{BF}_i = \frac{p(\mathbf{m}_i|\hat{\theta}_1, \text{“time-dependent model”})}{p(\mathbf{m}_i|\hat{\theta}_2, \text{“time-independent model”})}, \quad (16)$$

where $\hat{\theta}_1$ and $\hat{\theta}_2$ contain the maximum likelihood estimates of the hyperparameters in the corresponding BBGP models. Bayes factors indicate the degree of the models to be “time-dependent” rather than “time-independent”.

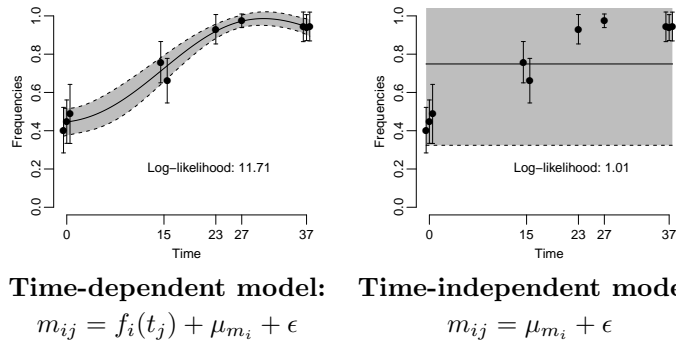


Figure 4: BBGP fits for the time-dependent and time-independent models for an example SNP taken from the real data set (Orozco-Ter Wengel *et al.*, 2012). Confidence regions are shown for ± 2 standard deviation. Similarly, error bars indicate ± 2 standard deviation (from FBB) interval. Replicates at the same time points are shifted by 0.5 for better visualisation. Maximum likelihood estimates of the parameters: $\hat{\theta}_1 = \{\hat{\ell} = 15.53, \hat{\sigma}_f^2 = 0.05, \hat{\sigma}_n^2 = 3.6 \times 10^{-8}\}$; $\hat{\theta}_2 = \{\hat{\sigma}_n^2 = 0.05\}$.

2.6 Cochran-Mantel-Haenszel Test

We compare BBGP against the Cochran-Mantel-Haenszel test (CMH), which was used by Orozco-Ter Wengel *et al.* (2012) to identify alleles with consistent allele frequency change across replicates. The CMH test has been proven to be the best-performing test statistic applied on HTS evolutionary data so far (Kofler and Schlötterer, 2014). Therefore, we take it as the basis of comparison with BBGP.

CMH allows to test whether the joint odds ratio of replicated ($r = 1, \dots, R$) allele counts in a $2 \times 2 \times R$ contingency table (Tab. 1) is significantly different from one. Significant deviation

| | Base gen. (B) | End gen. (E) | Σ |
|------------------|------------------|------------------|-----------------|
| SNP i allele 1 | $y_{iB_r}^{(1)}$ | $y_{iE_r}^{(1)}$ | $y_{i,r}^{(1)}$ |
| SNP i allele 2 | $y_{iB_r}^{(2)}$ | $y_{iE_r}^{(2)}$ | $y_{i,r}^{(2)}$ |
| Σ | n_{iB_r} | n_{iE_r} | $n_{i,r}$ |

Table 1: 2×2 contingency table of allele counts for the r -th replicate.

from one implies dependence of allele counts between two time points that is consistent among replicates. The CMH tests pairwise observations of the two alternative allele counts $y_{ij}^{(1)}$ and $y_{ij}^{(2)}$. In our bi-allelic case $y_{ij}^{(1)} = y_{ij}$ and $y_{ij}^{(2)} = n_{ij} - y_{ij}$. To compare the counts for all replicates $r = 1, \dots, R$ at the base (B) and the end (E) time points for each SNP position i , we denote $B_r = \{j | t_j = B, r_j = r\}$ and $E_r = \{j | t_j = E, r_j = r\}$. The CMH test statistic (see Agresti (2002) and Section A.1) compares the cell counts in Tab. 1 to their null expected values and it follows a chi-squared distribution with one degree of freedom $\chi_{(df=1)}^2$. We performed CMH tests on the simulated and real data for each SNP position independently, using the implementation of the software PoPoolation2 (Kofler *et al.*, 2011).

2.7 Simulations

To evaluate the performances of the BBGP and the CMH tests, we simulated data that mimics the dynamics of evolving *Dmel* populations at the genomic level. For this aim, we first simulated three sets of genome-scale data to evaluate the overall performances of the methods under the experimental design which is close to the natural settings. Additionally, we also carried out smaller size simulations on one chromosome arm to investigate the further influences of different parameter settings on the methods.

Whole-genome simulations We carried out forward Wright-Fisher simulations of genome-wide allele frequency trajectories of populations using the MimicEE simulation tool (Kofler and Schlötterer, 2014). The initial haplotypes were taken from Kofler and Schlötterer (2014) and they capture the natural variation of *Dmel* population. By sampling from the initial set, we established $r = 5$ replicated base populations using $H = 200$ founder haplotypes and let each of them evolve for $g = 60$ generations at a constant census size of $N = 1000$. We used the spatially varying recombination rate defined for *Dmel* by Fiston-Lavier *et al.* (2010). Low recombining regions were excluded from the simulations because of the elevated false positive rate in these regions (Kofler and Schlötterer, 2014). We followed the evolution of the total number of 1,939,941 autosomal SNPs among which 100 were selected with selection coefficient of $s = 0.1$ and semi-dominance ($h = 0.5$). Furthermore, we required the selected SNPs to have a starting frequency in the range $[0.12, 0.8]$, not to lose the minor allele in the course of time due to drift. We recorded the nucleotide counts for every second generation and performed Poisson sampling with $\lambda = 45$ (overall mean coverage in Orozco-Ter Wengel *et al.*, 2012) on the count data to produce coverage information (see Section A.2). We repeated the whole simulation experiment three times, each time using a different set of selected SNPs.

Single-chromosome-arm simulations For experimental design, additional simulations were carried out on a single chromosome arm ($\sim 16\text{Mb}$) with 25 selected SNPs to assess the performance under various parameter combinations, such as population size (N), number of founder haplotypes (H), selection coefficient (s), level of dominance (h), number of generations (g) and

number of replicates (r). We defined a basic set up with parameter space close to that of the whole genome simulations, i.e., $N = 1000, H = 200, r = 5, g = 60, s = 0.1, h = 0.5$, and investigated the effect on the performance when only one parameter is perturbed from its basic value.

2.8 Evaluation Metrics

The methods were evaluated based on precision, recall and average precision (AP) (Manning *et al.*, 2008). Precision and recall are commonly used metrics to measure the fraction of relevant items that are retrieved when comparing ranking based methods. Precision and recall are defined as

$$pre(k) = \frac{\text{number of selected SNPs in } k \text{ top SNPs}}{k}, \quad (17)$$

$$rec(k) = \frac{\text{number of selected SNPs in } k \text{ top SNPs}}{\text{number of selected SNPs}}. \quad (18)$$

The curve obtained by plotting the precision at every position in the ranked sequence of items as a function of recall is called the precision-recall curve. The area under the curve can be summarised using the average precision (Manning *et al.*, 2008), which is defined as the average of $pre(k)$ after every returned selected SNP:

$$aveP = \frac{\sum_{k=1}^N (pre(k) \mathbb{1}_{sel}(k))}{\text{number of selected SNPs}}, \quad (19)$$

where N is the total number of SNPs and

$$\mathbb{1}_{sel}(k) = \begin{cases} 1, & \text{if item at rank } k \text{ is a selected SNP,} \\ 0, & \text{otherwise.} \end{cases} \quad (20)$$

3 Results

3.1 Simulated Whole Genome Data

We applied the BBGP and CMH genome-wide on the simulated data with different numbers of time points (i.e., generations) and replicates. To evaluate the effect of the number of time points used, we tested the method using subsets of different sizes of the nine time points $\{0, 6, 14, 22, 28, 38, 44, 50, 60\}$ (see Section A.3 for details). We performed BBGP separately for each of the sampling schemes while CMH can only use two time points (first and last). All simulated SNPs were scored using Bayes factors for the BBGP, and p -values for the CMH test (e.g., see Fig. 8 for a graphical visualisation of the scores).

To investigate the effect of the number of replicates (r), we chose up to five replicates at each sampled time point. We first performed CMH tests with all possible r -replicate combinations. We then applied BBGP only to the best-performing replicate combinations of each size according to average precision in the CMH evaluations. This strategy ensures a fair comparison between the methods as BBGP is always evaluated against the best CMH results. We also compared BBGP to the standard GP of Kalaitzis and Lawrence (2011) that does not use the fixed beta-binomial model variances using the same replicate combinations as BBGP with 6 time points.

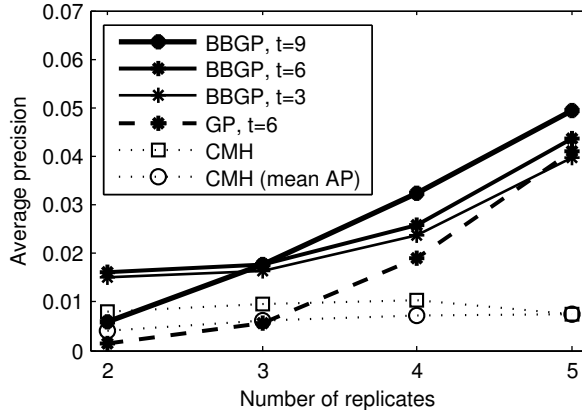


Figure 5: *Average precisions (AP) for CMH, BBGP, and standard GP with different number of replicates.* The used replicates have been selected as the best-performing r -replicate combinations in the CMH test, except for the CMH mean AP which has been computed by taking the mean of the average precisions over all r -replicate combinations for $r = 2, 3, 4, 5$. The corresponding precision-recall curves are shown in Figs. 9 and 10.

As shown in Fig. 5 (see also Fig. 9, Fig. 10), BBGP achieves a higher average precision than the standard GP and the CMH. Somewhat surprisingly, CMH seems to benefit very little from more replicates while the performance of the GP methods improves noticeably. The CMH is very sensitive to the specific replicates included, as including the fifth replicate in the optimal sequence actually leads to worse performance than four replicates (Fig. 10 (c-d)). We did not observe similar behaviour with the GP methods. On average over all possible r -replicate combinations, adding more replicates helps the CMH as well (mean AP in Fig. 5). The performance of the standard GP approaches that of BBGP as the number of replicates increases, which is consistent with the view that the stronger prior information from sequencing depth is most important when the data are otherwise scarce, as is often the case in real experiments. In contrast to more replicates, adding more time points improved the BBGP performance very little (Fig. 5).

We also investigated whether the two methods identify different types of selected SNPs. We calculated allele frequency change (AFC) for each SNP based on the average difference between the base and end populations across replicates. The CMH is very sensitive to large AFCs, while the candidates detected by the BBGP have a much more uniform distribution of AFCs (Fig. 12). In general, we would expect a uniform distribution of AFCs, as very large AFCs are only possible for SNPs with low starting frequency giving them the potential to rapidly increase. BBGP is much more accurate than CMH in all AFC classes as demonstrated by the performance breakdown in Fig. 13.

Furthermore, we performed a generalised CMH test (gCMH) that can be applied to more than two time points but requires a proper weighting scheme (Section A.1.1). As there is no straightforward way to find weights that accurately reflect natural selection, we used mid-ranks assigned to time points. With three time points, the gCMH does best, however, the performance drops with increasing number of time points (Fig. 14). We also see a precision decline as the number of replicates rises (Fig. 14), which is consistent with our previous observation that is the CMH is very sensitive to inconsistency among replicates.

The performance of the methods can vary noticeably between different experiments depending on their difficulty. For example, there is a 10-fold difference in AP between Experiment 1 and

Experiment 3 for both methods (Fig. 11, see also Kofler and Schlötterer (2014) for the CMH), but the BBGP-based test consistently outperforms the CMH test.

The running time needed to analyse 1000 SNPs in a 4 replicates- 6 time points setting is \approx 30 minutes on a desktop running Ubuntu 12.04 with Intel(R) Xeon(R) CPU E3-1230 V2 at 3.30GHz.

3.2 Influence of Parameter Choice

We have shown above that for simulated data with realistic parameters, our method can be applied on a genome-wide level. For the purpose of experimental design, we also investigated further parameter settings on the single chromosome arm of 2L.

3.2.1 Population size and number of founder haplotypes

In finite populations, genetic drift has a large impact on shaping the population allele frequencies. We studied the effect of census populations size (N) and the number of founder haplotypes (H) on our method. H can be thought as the number of different individuals (isofemale lines) in the base population. The populations were established by randomly choosing N individuals with replacement out of the H founders. The simulation results show that AP increases with increasing N (Fig. 6 (a)). This has also been observed by Kofler and Schlötterer (2014) for the CMH test. The AP is the highest with the ratio of $H/N = 0.5$ in all cases (Fig. 6 (a), Figs. 15-17) and the BBGP consistently outperforms the CMH test. Kofler and Schlötterer (2014) reported that the true positive rate for CMH test increases with H but the increment levels off with $H/N = 0.5$ for $N = 1000$. Baldwin-Brown *et al.* (2014) detected a constant increase in the power to localise a candidate SNP, however, they used a different method and investigated different parameter settings not comparable to ours. We hypothesise that as more low frequency variants are present in the population with $H/N > 0.5$, the selected SNPs with multiple linked backgrounds are competing with each other, resulting in an AP drop.

3.2.2 Selection strength and level of dominance

We investigated the performance using various selection coefficients (s) and fixed semidominance ($h = 0.5$). For moderate and strong selection ($s > 0.01$), the BBGP outperforms the CMH test (Figs. 6 (b), 18). The BBGP reaches the highest precision at $s = 0.1$, whereas the CMH test is the most precise at $s = 0.05$ which is consistent with Kofler and Schlötterer (2014). For strong selection ($s = 0.2$) the precision drops for both methods. The performance decay is presumably due to interference between selected sites, known as the Hill-Robertson effect, i.e., linkage between sites under selection will reduce the overall effectiveness of selection in finite populations (Hill and Robertson, 1966). Also, we hypothesise that long-range associations become more apparent as the strength of selection increases (Fig. 19) resulting in larger blocks rising in frequency together, which was also observed by Tobler *et al.* (2014).

For weak selection ($s \leq 0.01$), it becomes hard to distinguish between selection and drift in small populations. Thus, for low s , both methods perform rather poorly and the CMH has a slightly higher AP in these cases. However, for a more ideal parameter choice of $N = 5000$, $H = 2500$ and a long runtime of the experiment ($g = 120$), the BBGP gains a large performance improvement over the CMH test for $s = 0.01$ (see Figs. 20, 21) even in the difficult scenario of weak selection.

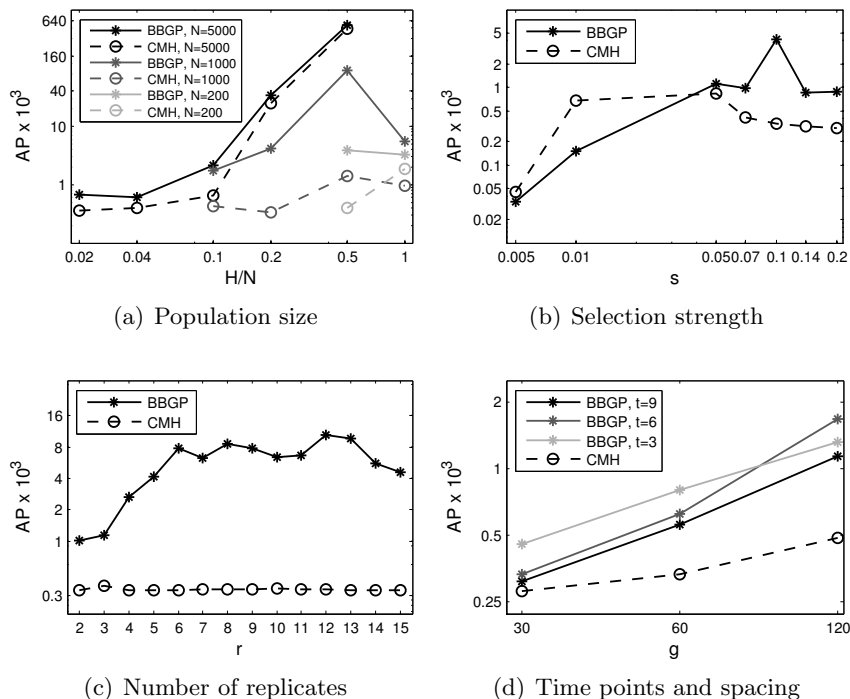


Figure 6: *Average precision for different experimental designs.* Log scale was used on both axes for (a), (b), (d), and on the y -axis for (c). Other parameters are as in the basic setup in Section 2.7.

We also simulated evolving populations using different level of dominance. The following relative fitness values were used on genotypes AA , Aa and aa : $w_{AA} = 1 + s$, $w_{Aa} = 1 + hs$, $w_{aa} = 1$, where $s = 0.1$. As the level of dominance (h) varies, we observed different behaviour of the methods. The AP of the CMH test increases as we are moving from complete recessivity ($h = 0$, recessive phenotype is selected) to complete dominance ($h = 1$, dominant phenotype is selected) (Figs. 22, 23). Selection on completely recessive allele results in a gradual initial change in AF with more rapid change in later generations and eventual fixation. On the other hand, the change in AF of a completely dominant allele is initially rapid but never reaches fixation since the recessive allele is shielded from natural selection in the heterozygote. When the fitness of the heterozygote is intermediate between the two homozygotes (additivity, $h = 0.5$) the allele frequency trajectory is the combination of the above mentioned ones, i.e., rapid initial change and quick fixation. BBGP reaches the highest AP with the additive scenario and relatively high AP in the recessive case (Fig. 22). When the dominant phenotype is selected ($h \sim 1$) and the unfavoured allele stays present in the population at low frequency, it is likely to result in an inconsistent behaviour of replicates, which lower the power of the BBGP.

3.2.3 Number of replicates

In addition to the whole-genome experiments with a maximum of 5 replicates, we simulated up to $r = 15$ replicates for the single chromosome arm. We observed a constant increase in performance for the BBGP up to $r = 6$ (Figs. 6(c), 24). The AP kept increasing up to $r = 12$ but rather in a fluctuating manner and then dropped with adding even more replicates. Consistently with the whole-genome simulations, we did not observe a large performance improvement with

increasing the number of replicates for the CMH test.

3.2.4 Length of the experiment and spacing of the samples

We also examined the performance with increasing the length of the experiments up to $g = 120$ generations. For longer experiments, more recombination events can happen, which uncouples linked sites letting them evolve independently. The AP rises rapidly for longer experiments (Figs. 6(d), 25). Thereby the performance gain is noticeably higher for the BBGP. We also investigated the spacing of the sampled time points ($t \in \{3, 6, 9\}$) for the BBGP and observed similar pattern that of the whole-genome simulations, i.e., an intermediate number of sample time points is sufficient as shape of selected trajectories is simple.

3.3 Real Data Application

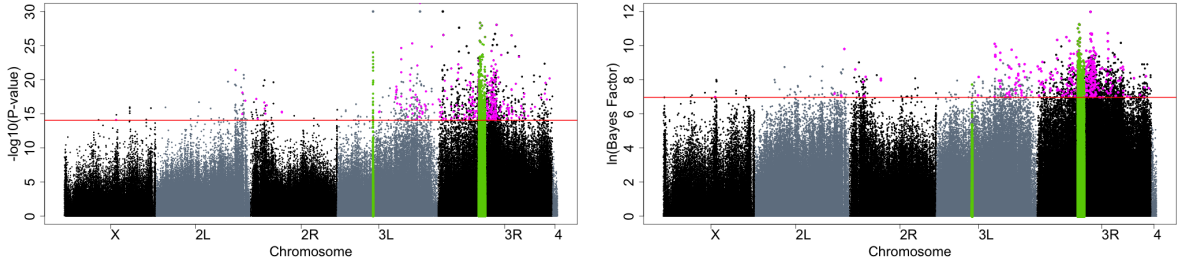
Orozco-Ter Wengel *et al.* (2012) applied the evolve and re-sequencing with HTS on *Dmel* populations adapting to elevated temperature regime to identify evolutionary trajectories of selectively favoured alleles. They established replicated base populations from isofemale lines collected in Portugal. The populations were propagated at a constant size of 1000 for 37 generations under fluctuating temperature regime (12h at 18 °C and 12h at 28 °C). DNA pool of 500 females (Pool-Seq) was extracted and sequenced in multiple replicates at the following time points: three replicates at the base generation 0 (B); two replicates at generation 15, an additional replicate at generation 23 and at generation 27; three replicates at the end generation 37 (E).

CMH tests were performed on a SNP-wise basis to identify significant allele frequency changes between the B and E populations (see Orozco-Ter Wengel *et al.* (2012) and Section A.4). We applied the BBGP method on 1,547,765 SNPs from the experiment and compared the results with that of the B-E comparison of the CMH test. The overlap between the top 2000 candidate SNPs of the CMH and the BBGP was rather small (524 SNPs). However, the peaks of both methods covered the same regions (Fig. 7). Using a gene set enrichment analysis (see Section A.5), we also found that the top ranked significantly enriched Gene Ontology categories were similar for both tests (Tabs. 4, 5, Fig. 26). Furthermore, Fig. 7 shows how well the posterior beta-binomial variance inference can handle false signals resulting from uneven coverage. While the CMH test is misled by strong signal coming from high coverage of the chorion cluster with high copy number variation, the BBGP test does not falsely indicate signatures of selection (Fig. 7, green region on 3L).

Although *Dmel* generally has rather small levels of linkage, linkage disequilibrium (LD) might have built up during the course of the experiment. In fact, LD had a major effect on the number of candidate SNPs identified by the CMH as well as the BBGP based test. As the flanking SNPs showed signs of hitchhiking, the observed AFC of the flanking SNPs were also significant (see also Manhattan plot for the simulated SNPs, Fig. 8) and this made it difficult to narrow down functionally important regions for thermoadaptation.

4 Discussion

Our results in detecting SNPs that are evolving under selection using a GP model clearly demonstrate the importance of careful modelling of the measurement uncertainty through a good noise model, in our case using the beta-binomial model of sequencing data. Especially when



(a) Genome-wide distribution of CMH $-\log(p\text{-values})$. (b) Genome-wide distribution of BBGP $\ln(\text{Bayes factor})$.

Figure 7: *Manhattan plots of genome-wide SNP-values.* (a) $-\log_{10}(p\text{-values})$ for the CMH test B-E comparison. p -values below $1e-30$ were clipped to $1e-30$ on the plot. (b) $\ln(\text{Bayes factor})$ for the BBGP. Only those SNPs are indicated for which we calculated both the p -values and the Bayes factors (we did not infer Bayes factors for fixed SNPs). A 1 Mb region was excluded from the analysis on 3R as a low frequency haplotype spreads during the experiment. Previously, the chorion gene cluster on 3L was also excluded as this region has extremely high coverage (Orozco-Ter Wengel *et al.*, 2012). Regions that were excluded from the analysis are shown in green. The red horizontal line indicates the top 2000 candidate cutoff. The common candidates among the top 2000 are highlighted in magenta. Figure (b) shows how well the beta-binomial variance control can handle high coverage problem of the excluded region on 3L.

data are scarce, the BBGP approach leads to much higher accuracy than standard maximum likelihood estimation of noise variances. Incorporating the non-Gaussian likelihood directly to the GP would also be possible, but it would lead to computationally more demanding inference.

In terms of experimental design, the most effective way to improve performance is to use a larger population (N) and a larger number of founder haplotypes (H). As expected, alleles under moderate to strong selection ($s = 0.05-0.1$) are easier to detect than alleles changing under weak selection ($s \leq 0.01$). However, for very strong selection ($s \geq 0.2$), it is again hard to detect the causal SNPs. In a real experiment the strength of selection might also not be known and often cannot be changed for the trait of interest.

Adding more replicates can also help improve performance up to some point. Compared to the CMH test, the BBGP is clearly superior in utilising additional replicates. We suspect this is because CMH assumes all replicates should have similar odds ratios between the two time points and this is not sufficiently satisfied by the noisy data. Longer experiments can help significantly (Fig. 20), but the benefit of adding more intermediate time points seems smaller. This may be because the shape of selected trajectories is a simple sigmoid and adding more points provides limited help in estimating them.

The presented GP-based test is sensitive to SNPs with a consistent time-varying profile. A statistically more accurate model could be derived by assuming each replicate to follow an independent GP, but this would require different kind of constraints to differentiate between selection and drift, which may be difficult to formulate for multiple interacting SNPs which do not follow a simple parametric model. Exploring hierarchical GP models to capture the correct dependence structure in a sensible test is an interesting avenue of future research.

In a whole-genome experiment, linkage disequilibrium between nearby markers and interactions between nearby selected SNPs are important confounders in identifying the selected markers.

Based on our simulations, we believe that especially for moderate-sized populations the interactions can be quite problematic, leading to very large segments in the genome raising together in frequency (Fig. 19). The issue does not appear when simulating only a single selected SNP (Fig. 27), which strongly suggests it is caused by the interactions. The issue can be most effectively mitigated by using larger populations (Fig. 28 (c-d)). An artificially high recombination rate (Fig. 28 (a-b)) could also break the interactions. Working with larger fixed window sizes might not improve the performance as a substantial number of hitchhikers can still be found hundreds of kb from the selected SNPs (See Fig. 29: The removal of nearby hitchhikers did not improve the average precision noticeably). It is possible to extend the GP models for joint analysis of multiple SNPs, and this is clearly an important avenue of future research. This is potentially a further advantage of the GP, because it is much more difficult to similarly extend the frequentist tests.

5 Conclusion

In this paper, we developed a new test that is based on combining GP models with a beta-binomial model of sequencing data, and compared it with the CMH test that allows the pairwise comparison of base and evolved populations across several replicates.

Our results demonstrate that GP models are well-suited for analysing quantitative genomic time series data because they can effectively utilise the available data, making good use of additional time points and replicates unhindered by uneven sampling and consistently show performance superior to the CMH test.

The GP framework is very flexible which enables extensions utilising for example linkage disequilibrium over nearby alleles. As GP models can easily incorporate additional information on the data, we envisage that further promising combinations of the GP approach with evolutionary models will emerge.

Acknowledgement

C.K. would like to thank the Institute of Pure and Applied Mathematics (IPAM) for a stay at the Genomics programme at which the idea of working on evolutionary time series data evolved.

Funding: The work was supported under the European ERASysBio+ initiative project “SYNERGY” through the Academy of Finland [135311]. A.H. was also supported by the Academy of Finland [259440] and H.T. was supported by Alfred Kordelin Foundation. A.J. is member of the Vienna Graduate School of Population Genetics which is supported by a grant of the Austrian Science Fund (FWF) [W1225-B20].

References

- Agresti, A. (2002). *Categorical Data Analysis*. Wiley, New York.
- Äijö, T et al. (2013). Sorad: a systems biology approach to predict and modulate dynamic signaling pathway response from phosphoproteome time-course measurements. *Bioinformatics*, **29**(10), 1283–1291.
- Ashburner, M et al. (2000). Gene ontology: tool for the unification of biology. *Nat Genet*, **25**(1), 25–29.

- Baldwin-Brown, JG et al. (2014). The power to detect quantitative trait loci using resequenced, experimentally evolved populations of diploid, sexual organisms. *Mol Biol Evol*, **31**(4), 1040–1055.
- Barrick, JE et al. (2009). Genome evolution and adaptation in a long-term experiment with *Escherichia coli*. *Nature*, **461**(7268), 1243–1247.
- Bollback, JP et al. (2008). Estimation of $2N_e$ s from temporal allele frequency data. *Genetics*, **179**(1), 497–502.
- Burke, M et al. (2010). Genome-wide analysis of a long-term evolution experiment with *Drosophila*. *Nature*, **467**, 587–590.
- Burke, M. K. and Long, A. (2012). What paths do advantageous alleles take during short-term evolutionary change? *Molecular Ecology*, **21**, 4913–416.
- Cooke, EJ et al. (2011). Bayesian hierarchical clustering for microarray time series data with replicates and outlier measurements. *BMC Bioinformatics*, **12**, 399.
- Fiston-Lavier, AS et al. (2010). *Drosophila melanogaster* recombination rate calculator. *Gene*, **463**(1-2), 18–20.
- Friendly, M. (2014). *vcdExtra: vcd extensions and additions*. R package version 0.6-0.
- Gao, P et al. (2008). Gaussian process modelling of latent chemical species: applications to inferring transcription factor activities. *Bioinformatics*, **24**(16), i70–i75.
- Hensman, J et al. (2013). Hierarchical Bayesian modelling of gene expression time series across irregularly sampled replicates and clusters. *BMC Bioinformatics*, **14**, 252.
- Hill, W. G. and Robertson, A. (1966). The effect of linkage on limits to artificial selection. *Genet Res*, **8**(3), 269–294.
- Honkela, A et al. (2010). Model-based method for transcription factor target identification with limited data. *Proc Natl Acad Sci U S A*, **107**(17), 7793–7798.
- Illingworth, CJR et al. (2012). Quantifying selection acting on a complex trait using allele frequency time series data. *Mol Biol Evol*, **29**(4), 1187–1197.
- Jones, N. S. and Moriarty, J. (2013). Evolutionary inference for function-valued traits: Gaussian process regression on phylogenies. *J R Soc Interface*, **10**(78), 20120616.
- Kalaitzis, A. A. and Lawrence, N. D. (2011). A simple approach to ranking differentially expressed gene expression time courses through Gaussian process regression. *BMC Bioinformatics*, **12**, 180.
- Kawecki, TJ et al. (2012). Experimental evolution. *Trends Ecol Evol*, **27**(10), 547–560.
- Kimura, M. (1962). On the probability of fixation of mutant genes in a population. *Genetics*, **47**, 713–719.
- Kirk, P. D. W. and Stumpf, M. P. H. (2009). Gaussian process regression bootstrapping: exploring the effects of uncertainty in time course data. *Bioinformatics*, **25**(10), 1300–1306.
- Kofler, R. and Schlötterer, C. (2012). Gowinda: unbiased analysis of gene set enrichment for genome-wide association studies. *Bioinformatics*, **28**, 2084–2085.
- Kofler, R. and Schlötterer, C. (2014). A guide for the design of evolve and resequencing studies. *Mol Biol Evol*, **31**(2), 474–483.
- Kofler, R et al. (2011). PoPoolation2: identifying differentiation between populations using sequencing of pooled DNA samples (Pool-Seq). *Bioinformatics*, **27**, 3435–3436.
- Kuritz, SJ et al. (1988). A general overview of mantel-haenszel methods: applications and recent developments. *Annu Rev Public Health*, **9**, 123–160.
- Lang, GI et al. (2013). Pervasive genetic hitchhiking and clonal interference in forty evolving yeast populations. *Nature*, **500**(7464), 571–574.
- Liu, Q et al. (2010). Estimating replicate time shifts using Gaussian process regression. *Bioinformatics*, **26**(6), 770–776.
- Liu, W. and Niranjana, M. (2012). Gaussian process modelling for bicoid mRNA regulation in spatio-temporal Bicoid profile. *Bioinformatics*, **28**(3), 366–372.
- Manning, CD et al. (2008). *Introduction to Information Retrieval*. Cambridge University Press.
- Orozco-Ter Wengel, P et al. (2012). Adaptation of *Drosophila* to a novel laboratory environment reveals temporally heterogeneous trajectories of selected alleles. *Molecular Ecology*, **21**, 4931–4941.
- Palacios, J. A. and Minin, V. N. (2013). Gaussian process-based Bayesian nonparametric inference of population size trajectories from gene genealogies. *Biometrics*, **69**(1), 8–18.
- Rasmussen, C. E. and Williams, C. K. I. (2006). *Gaussian Processes for Machine Learning*. The MIT Press.

- Segrè, A et al. (2010). Common inherited variation in mitochondrial genes is not enriched for associations with type 2 diabetes or related glycemic traits. *PLoS Genet.*, **6**, e1001058. doi:10.1371/journal.pgen.1001058.
- Stegle, O et al. (2010). A robust Bayesian two-sample test for detecting intervals of differential gene expression in microarray time series. *J Comput Biol*, **17**(3), 355–367.
- Titsias, MK et al. (2012). Identifying targets of multiple co-regulating transcription factors from expression time-series by Bayesian model comparison. *BMC Syst Biol*, **6**, 53.
- Tobler, R et al. (2014). Massive habitat-specific genomic response in *D. melanogaster* populations during experimental evolution in hot and cold environments. *Mol Biol Evol*, **31**(2), 364–375.
- Turner, T et al. (2011). Population-based resequencing of experimentally evolved populations reveals the genetic basis of body size variation in *Drosophila melanogaster*. *PLoS Genetics*, **7**(3), e1001336.
- Yuan, M. (2006). Flexible temporal expression profile modelling using the Gaussian process. *Comput. Statist. Data Anal.*, **51**(3), 1754–1764.
- Zhou, D et al. (2011). Experimental selection of hypoxia-tolerant *Drosophila melanogaster*. *Proceedings of the National Academy of Sciences*, **7**(108), 2349–2354.

A Supplementary Methods

A.1 Cochran-Mantel-Haenszel Test

SNPs with consistent change in allele frequency were identified with Cochran-Mantel-Haenszel test (CMH) by Orozco-Ter Wengel *et al.* (2012). The CMH test is an extension of testing equivalence of proportions (implies that the odds ratio is 1) in a 2×2 contingency table to replicated tables sampled from the same underlying population. The estimate for the joint odds ratio in the replicated $2 \times 2 \times R$ tables ($r = 1, \dots, R$, Tab. 1) is tested for difference from 1.

We follow the definition of the CMH by Agresti (2002). Allele counts for the different replicates ($y_{iB_r}^{(1)}$, Tab. 1) are assumed to be independent. Under the null hypothesis, they follow a hypergeometric distribution with mean and variance:

$$E(y_{iB_r}^{(1)}) = \frac{y_{i,r}^{(1)} n_{iB_r}}{n_{i,r}}$$

$$V(y_{iB_r}^{(1)}) = \frac{y_{i,r}^{(1)} y_{i,r}^{(2)} n_{iB_r} n_{iE_r}}{n_{i,r}^2 (n_{i,r} - 1)}.$$

The test statistic compares $\sum_r y_{iB_r}^{(1)}$ to its null expected value by combining information from R partial tables:

$$CMH = \frac{\left[\sum_r \left(y_{iB_r}^{(1)} - E(y_{iB_r}^{(1)}) \right) \right]^2}{\sum_r Var \left(y_{iB_r}^{(1)} \right)}.$$

This statistic approximately follows a chi-square distribution with one degree of freedom $\chi_{(df=1)}^2$. Under the null hypothesis, we assume independence of the start (B) and end (E) time points of the experiment for each replicate. Thus, the odds ratio for each replicate is approximately one. When the odds ratio in each partial table is significantly different from one (dependence) we expect the nominator in the test statistic to be large in absolute value.

A.1.1 Generalized Cochran-Mantel-Haenszel Test (gCMH)

The CMH tests for associations between pairwise allele counts and it is not able to handle time serial data. However, it can be generalized for $K \times L \times R$ contingency tables (Kuritz *et al.*, 1988) where the null hypothesis of no partial association between the row ($i = 1, \dots, K$) dimensions and column ($j = 1, \dots, L$) dimensions for all replicates ($r = 1, \dots, R$) is tested. Similarly to the CMH test, under the null hypothesis the cell counts do not deviate from their expected value under random association. The alternative hypothesis can vary depending on whether the row and column variables are measured in the nominal or ordinal scale. In the HTS allele frequency data, the row variable (allele A and B) is nominal, whereas the column variable (allele counts at different time points) is measured on the ordinal scale. We test the alternative hypothesis that mean allele frequency across several time points differ between alleles. Mean allele frequencies are formed by assigning (column) scores to time points and the difference between the weighted mean scores across rows are tested (see e.g. Kuritz *et al.* (1988) for details). There is no straightforward way to find a proper weighting scheme of the time points, which accurately

reflects the action of natural selection. We used the R implementation of the generalized CMH test in `vcdExtra` (Friendly, 2014) package where mid-ranks can be assigned to column scores (`cscores="midrank"`). Using these marginal ranks obtained from each table, the test statistic is equivalent to an extension of Kruskal-Wallis analysis of variance test on ranks.

To our knowledge, the gCMH test has not been used to analyse HTS allele frequency data. We used it on our simulated whole-genome data set to see if performance improvement can be achieved when time serial information is incorporated to the CMH test. We performed gCMH with increasing number of replicates using $t = 3, 6, 9$ time points (Fig. 14). With less time points ($t = 3$, Fig. 14 (a)) the gCMH does better but the performance drops with increasing the number of time points. Generally, we also see a precision decline as the number of replicates rises.

A.2 Simulations

We carried out whole-genome forward Wright-Fisher simulations of allele frequency (AF) trajectories of evolving populations with `MimicrEE` (Kofler and Schlötterer, 2014). The founder population was generated using 8000 simulated haploid genomes from Kofler and Schlötterer (2014). Out of the 8000 genomes, 200 were sampled to establish a diploid base population of 1000 individuals (sampled out of the 200 with replacement). The base population contains only autosomal SNPs. Low recombining regions ($< 1cM/Mb$) were also excluded from the simulations (for more information see Kofler and Schlötterer, 2014). We randomly placed 100 selected SNPs in the base population with selection coefficient of $s = 0.1$ and semi-dominance ($h = 0.5$). The selected SNPs have a starting allele frequency in the range $[0.12, 0.8]$. We applied this restriction on the starting AF to increase the probability of fixation of the selected allele. According to population genetics theory, the probability of fixation is $P_{fix} = (1 - e^{-2N_e s p}) / (1 - e^{-2N_e s})$ (Kimura, 1962), where N_e is the effective population size, s is the selection coefficient and p is the starting allele frequency. Taking the base population of 1000 homozygote individuals and the set of selected SNPs, we followed the simulation protocol outlined at <https://code.google.com/p/mimicree/wiki/ManualMimicrEESummary> for 5 replicates independently. As described in Kofler and Schlötterer (2014), we aimed to reproduce the sampling properties of Pool-Seq using Poisson sampling with $\lambda = 45$ (using the script `poisson-3fold-sample.py` available at <http://mimicree.googlecode.com>). Briefly, we considered coverage differences between samples, coverage fluctuations due to GC-bias and stochastic sampling heterogeneity.

A.3 Performance tests on simulated data

We measured the performance of the BBGP and the CMH test using whole-genome simulated data with various number of time points and replicates. To evaluate the effect of the number of time points used, the following sampling schemes were carried out. We started with nine time points $\{0, 6, 14, 22, 28, 38, 44, 50, 60\}$ and then removed the midpoint of the shortest interval until the desired number of time points was achieved. In the case of a tie, we kept the time point which is closest to the real sequenced time points in Orozco-Ter Wengel *et al.* (2012). Following this rule, we applied BBGP on the following sets of generations:

- 3 time points: 0, 38, 60,
- 4 time points: 0, 14, 38, 60,

- 5 time points: 0, 14, 28, 38, 60,
- 6 time points: 0, 14, 28, 38, 50, 60,
- 7 time points: 0, 14, 22, 28, 38, 50, 60,
- 8 time points: 0, 6, 14, 22, 28, 38, 50, 60,
- 9 time points: 0, 6, 14, 22, 28, 38, 44, 50, 60.

For the CMH test, however, we always performed a base-end (generation 60) comparison, because the CMH is a pairwise statistic. The genome-wide test statistic values are shown in Fig. 8 for the BBGP (6 time points) and the CMH for 5 replicates as an example. The effects of different numbers of replicates on the performance of the proposed methods are shown in Fig. 10 using precision recall curves along with average precisions.

We carried out 3 independent runs of simulations with different sets of selected SNPs but keeping the parameters unchanged (Fig. 11). Finally, we compared with a performance break down according to Allele Frequency Change (AFC) the BBGP to CMH test in different AFC classes (Fig. 12 and Fig. 13).

A.3.1 Tests of parameter choice for experimental design

We investigated different choices of parameters for experimental design. As whole-genome simulations are computationally very demanding, we decided to simulate only a single chromosome arm (2L) with 25 selected SNPs using various parameter settings. This reduces the running times significantly, but the length of the genome segment ($\sim 16Mb$) and the number of selected SNPs used are still realistic proxy to the performance on the whole-genome. We report performance results for different population size - number of founder haplotypes ($\frac{H}{N}$ combinations (Figs. 15-17), for various selection coefficients s (Figs. 18- 21), levels of dominance h (Figs. 22, 23), increasing number of replicates r (Fig. 24) and the choice of time points at different intermediate generations g (Fig 25).

A.4 Real Data Application

We applied the BBGP on HTS data of experimentally evolved *D. melanogaster* populations (Orozco-Ter Wengel *et al.*, 2012). We compared our proposed method to the CMH results coming from the B-E comparison, downloaded from Dryad database (<http://datadryad.org>) under the accession: doi: 10.5061/dryad.60k68. We used the synchronized pileup files (BF37.sync) which contains a total number of 1,547,837 SNPs. The CMH test was only performed on SNPs that met certain quality criteria regarding the minor allele count and the maximum coverage (for more information on SNP calling please consult Orozco-Ter Wengel *et al.*, 2012).

A.5 Gene Set Enrichment

We used gene set enrichment to test for significantly enriched functional categories according to the Gene Ontology (GO) database (Ashburner *et al.*, 2000). Orozco-Ter Wengel *et al.* (2012) used Gowinda (Kofler and Schlötterer, 2012) to test significance of overrepresentation of candidate SNPs in each GO category. Gowinda uses permutation tests to eliminate potential sources of bias caused by difference of gene length and genes that overlap (explained below). We tested the top 2000 candidate SNPs for both the CMH and the BBGP methods, respectively. FDR

correction was applied on the inferred p -values to account for multiple testing. Using Gowinda, we did only find one significantly enriched category ($p < 0.05$) for the BBGP and no significant categories for the CMH test (see Tables 2 and 3).

In addition to taking an arbitrary threshold of the top 2000 SNPs, we also considered the full distributions of p -values for the CMH and the distribution of Bayes factors for the BBGP based tests. For each GO category we compared distribution of all SNP-values (p -values for the CMH and Bayes factors for the GP) in that GO gene set to the distribution outside that gene set using a one-tailed Mann-Whitney U test (MWU) as applied by Segrè *et al.* (2010). Similar to Gowinda, we used permutations to account for biases such as gene length and other confounding effects (see below). We also conserve the gene order during the randomization as functionally similar genes are often clustered nearby on a chromosome. Using the MWU tests, we found significant GO category enrichments for both methods (Fig. 26). Moreover, the top ranked candidate categories were similar in both cases (see Tabs. 4, 5).

A.5.1 Gene Set Enrichment with Gowinda

Gowinda counts the number of genes (set of candidate genes) that contain candidate SNPs. Assuming that SNPs are in complete linkage within the same gene, it randomly samples SNPs from the pool of all SNPs until the number of corresponding genes is equal to the cardinality of the set of candidate genes. This step is repeated several times and from the resulting random set of genes, an empirical null distribution of candidate gene abundance is calculated for each gene set. The significance level of enrichment for each gene set is inferred by counting the randomly drawn cases, in which there were more candidate genes present than in the original candidate gene set. Gowinda requires the following input files: annotation file containing the annotation of species of interest; gene set file of the associated genes (e.g. Gene Ontology (GO) association file); list of SNP-value pairs as the output of our analysis; list of candidate SNPs, which is a subset of all SNP-value pairs that we define as candidates according to some predetermined condition. We used the following inputs: the annotation file of *Drosophila melanogaster* version 5.40 downloaded from Flybase (<http://flybase.org/>); the GO association file was obtained from R Bioconductor GO.db package version 2.9.0 (accessed at 05/03/2013). We took the top 2000 candidate SNPs for both methods as candidate SNPs and run Gowinda with the following parameters: `--simulations 10000000 --gene-definition updownstream200 --mode gene`. We also took 200 base pairs up- and downstream regions from the gene boundaries into the analysis. For more details please see Kofler and Schlötterer (2012).

Using Gowinda led to only one significantly enriched category for the BBGP and no significant enrichment for the CMH test ($FDR < 0.05$; top ranked categories in Tab. 2 and Tab. 3).

A.5.2 Gene Set Enrichment with Mann-Whitney U Test

For using Gowinda, we had to fix a threshold above which we consider a SNP as a possible candidate. Defining this threshold can be arbitrary, and changes in the threshold can result in different enriched gene sets. Therefore, we decided to compare the distribution of all SNP-values in a specific gene set to the distribution outside that gene set using Mann-Whitney U test (MWU). This test allows us to decide if a particular gene set is significantly enriched based only on the ranks of SNP-values in that set.

We performed the MWU test similarly as Segrè *et al.* (2010). We used the previously mentioned gene set file obtained from R Bioconductor GO.db package; and a list of all SNPs with the

corresponding values (output of the tests). For mapping the SNPs to the genes we used SNPEFF 2.0.1 (<http://snpeff.sourceforge.net/>). For each gene set we summarized the list of SNPs present in that particular set and created a vector of corresponding SNP-values (list of p -values or Bayes factors). Then we tested the alternative hypothesis that the distribution of these values is skewed towards the extreme values (low ranked p -values for the CMH, high ranked Bayes factors for the GP) compared to the values among the rest of the SNPs. This gives the observed rank-sum p -value for the investigated gene set. Then, similarly to Gowinda, we performed permutations to account for biases by simulating random gene sets (but keeping the chromosomal order) with identical size as observed. For every round of simulation, we calculated the ranked-sum p -values as before. Finally, an expected rank-sum p -value was computed from this null distribution, as the fraction of randomly sampled gene sets whose rank-sum p -value was less than or equal to the observed rank-sum p -value of the gene set.

The top ranked significant enrichments calculated with MWU test using 1000 permutations are functionally rather similar. Fig. 26 shows the overlap between highly enriched categories for different empirical p -value cutoffs. The categories are listed in Tab. 4 and Tab. 5.

B Supplementary Tables and Figures

| GO category | p -Value | FDR | Description |
|-------------|------------|-------------|-------------------------------------|
| GO:0004003 | 0.000074 | 0.0630949 | ATP-dependent DNA helicase activity |
| GO:0008094 | 0.0001048 | 0.0630949 | DNA-dependent ATPase activity |
| GO:0006281 | 0.0002248 | 0.097873567 | DNA repair |
| GO:0046914 | 0.000305 | 0.1027073 | transition metal ion binding |

Table 2: *Top ranked GO enrichment results with Gowinda on the CMH candidates.* Only the top 4 categories are shown.

| GO category | p -Value | FDR | Description |
|-------------|------------|-------------|------------------------------------|
| GO:0005506 | 0.0000143 | 0.015987 | iron ion binding |
| GO:0015671 | 0.0004199 | 0.256548725 | oxygen transport |
| GO:0004252 | 0.0006096 | 0.256548725 | serine-type endopeptidase activity |
| GO:0004989 | 0.0007332 | 0.256548725 | octopamine receptor activity |

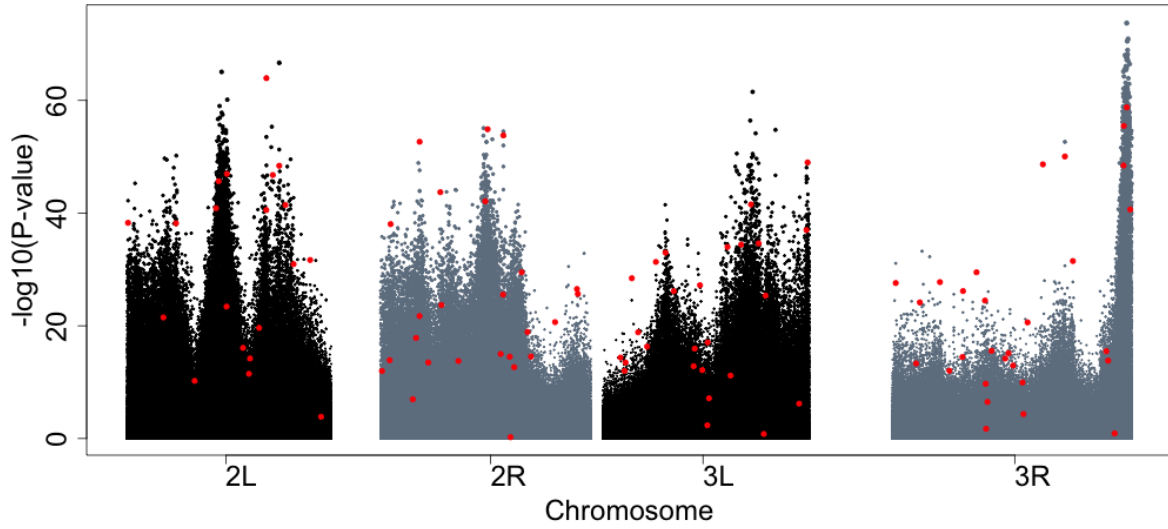
Table 3: *Top ranked GO enrichment results with Gowinda on the BBGP candidates.* Only the top 4 categories are shown.

| GO category | Obs. p-val. | Emp. p-val. | Description |
|-------------|----------------|----------------|--|
| GO:0007274 | 2.8543e-156 | 0.001 | neuromuscular synaptic transmission |
| GO:0032504 | 3.2726e-49 | 0.001 | multicellular organism reproduction |
| GO:0006997 | 1.2159e-17 | 0.001 | nucleus organization |
| GO:0007379 | 4.9304e-75 | 0.008 | segment specification |
| GO:0003774 | 1.8303e-19 | 0.011 | motor activity |
| GO:0009792 | 5.8937e-30 | 0.013 | embryo development ending in birth or egg hatching |
| GO:0001700 | 9.7049e-31 | 0.015 | embryonic development via the syncytial blastoderm |
| GO:0045451 | 4.5162e-20 | 0.015 | pole plasm oskar mRNA localization |
| GO:0060810 | 2.3554e-19 | 0.015 | intracell. mRNA loc. inv. in pattern specification proc. |
| GO:0060811 | 1.9679e-19 | 0.016 | intracell. mRNA loc. inv. in anterior/posterior axis spec. |
| GO:0000975 | 1.5011e-32 | 0.017 | regulatory region DNA binding |
| GO:0008298 | 5.7685e-17 | 0.017 | intracellular mRNA localization |
| GO:0016573 | 3.4293e-08 | 0.024 | histone acetylation |
| GO:0019094 | 6.8648e-19 | 0.025 | pole plasm mRNA localization |
| GO:0060438 | 9.6931e-101 | 0.026 | trachea development |
| GO:0000086 | 1.0455e-15 | 0.027 | G2/M transition of mitotic cell cycle |
| GO:0030554 | 9.0394e-19 | 0.028 | adenyl nucleotide binding |
| GO:0051049 | 4.8523e-52 | 0.029 | regulation of transport |
| GO:0004386 | 1.9648e-09 | 0.029 | helicase activity |
| GO:0007093 | 6.4409e-08 | 0.029 | mitotic cell cycle checkpoint |
| GO:0032879 | 3.4419e-34 | 0.03 | regulation of localization |
| GO:0060439 | 6.0698e-78 | 0.032 | trachea morphogenesis |
| GO:0019904 | 3.6125e-74 | 0.032 | protein domain specific binding |
| GO:0007350 | 1.1101e-25 | 0.033 | blastoderm segmentation |
| GO:0000976 | 3.9652e-14 | 0.035 | transcr.regulatory reg. sequence-spec. DNA binding |
| GO:0000977 | 2.8459e-28 | 0.037 | RNA polymerase II reg. reg.seq.-spec. DNA binding |
| GO:0007276 | 3.7400e-24 | 0.038 | gamete generation |
| GO:0007269 | 1.1198e-94 | 0.04 | neurotransmitter secretion |
| GO:0004888 | 2.9136e-19 | 0.043 | transmembrane signaling receptor activity |
| GO:0000981 | 1.9244e-28 | 0.044 | seq.-spec DNA binding RNA pol. II transcr. factor activity |
| GO:0008306 | 1.2419e-35 | 0.046 | associative learning |
| GO:0008355 | 6.2395e-32 | 0.047 | olfactory learning |
| GO:0001012 | 1.3174e-37 | 0.048 | RNA polymerase II regulatory region DNA binding |
| GO:0048149 | 1.6131e-23 | 0.048 | behavioral response to ethanol |
| GO:0045664 | 7.9648e-23 | 0.048 | regulation of neuron differentiation |
| GO:0010389 | 1.8391e-08 | 0.05 | regulation of G2/M transition of mitotic cell cycle |
| GO:0009055 | 7.5572e-05 | 0.05 | electron carrier activity |

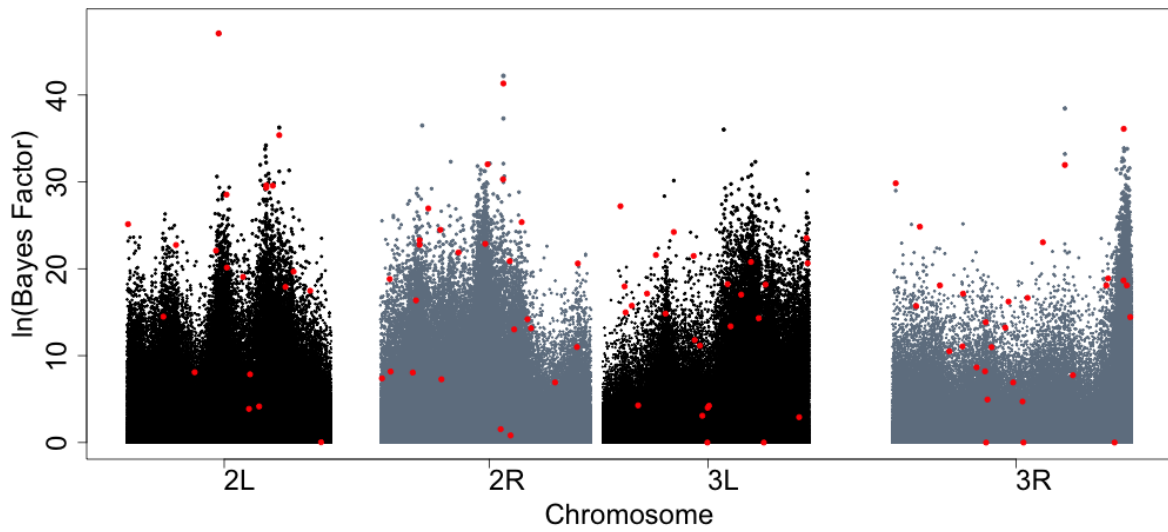
Table 4: *Results of the GO enrichment with MWU on the CMH candidates.* Only the categories are shown for which the empirical p -value ≤ 0.05 calculated for 1000 permutations.

| GO category | Obs. p-val. | Emp. p-val. | Description |
|-------------|----------------|----------------|---|
| GO:0006997 | 4.1404e-19 | 0 | nucleus organization |
| GO:0007274 | 1.0657e-130 | 0.002 | neuromuscular synaptic transmission |
| GO:0007379 | 3.7449e-85 | 0.002 | segment specification |
| GO:0032879 | 8.0269e-38 | 0.006 | regulation of localization |
| GO:0000075 | 1.9450e-19 | 0.007 | cell cycle checkpoint |
| GO:0000785 | 9.1310e-15 | 0.014 | chromatin |
| GO:0051049 | 6.3596e-52 | 0.019 | regulation of transport |
| GO:0009152 | 2.7329e-41 | 0.02 | purine ribonucleotide biosynthetic process |
| GO:0006164 | 5.9106e-46 | 0.022 | purine nucleotide biosynthetic process |
| GO:0004386 | 1.0113e-09 | 0.025 | helicase activity |
| GO:0005179 | 1.9714e-16 | 0.026 | hormone activity |
| GO:0000975 | 2.2740e-25 | 0.027 | regulatory region DNA binding |
| GO:0000977 | 9.8625e-36 | 0.028 | RNA pol. II regulatory reg. seq.-spec. DNA binding |
| GO:0000976 | 2.6106e-18 | 0.029 | transcr. reg. region sequence-spec.DNA binding |
| GO:0001012 | 2.0242e-42 | 0.029 | RNA polymerase II regulatory region DNA binding |
| GO:0030554 | 1.9638e-14 | 0.03 | adenyl nucleotide binding |
| GO:0046914 | 5.2243e-27 | 0.032 | transition metal ion binding |
| GO:0055114 | 7.0135e-18 | 0.032 | oxidation-reduction process |
| GO:0005829 | 1.0637e-17 | 0.033 | cytosol |
| GO:0019725 | 2.3293e-26 | 0.034 | cellular homeostasis |
| GO:0032504 | 8.4897e-21 | 0.036 | multicellular organism reproduction |
| GO:0009165 | 8.8494e-25 | 0.038 | nucleotide biosynthetic process |
| GO:0008285 | 7.1838e-19 | 0.041 | negative regulation of cell proliferation |
| GO:0007269 | 1.6094e-94 | 0.043 | neurotransmitter secretion |
| GO:0010389 | 3.4665e-07 | 0.043 | regulation of G2/M transition of mitotic cell cycle |
| GO:0031226 | 5.5250e-27 | 0.043 | intrinsic to plasma membrane |
| GO:0032940 | 3.7154e-73 | 0.045 | secretion by cell |
| GO:0017076 | 5.6881e-12 | 0.046 | purine nucleotide binding |
| GO:0000086 | 5.0627e-14 | 0.048 | G2/M transition of mitotic cell cycle |
| GO:0016491 | 1.1667e-10 | 0.048 | oxidoreductase activity |

Table 5: Results of the GO enrichment with MWU on the BBGP candidates. Only the categories are shown for which the empirical p -value ≤ 0.05 calculated for 1000 permutations.

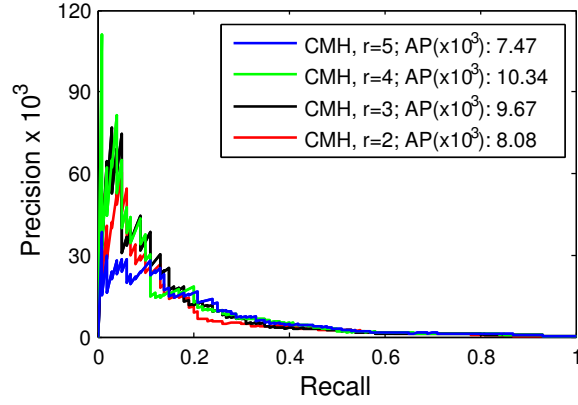


(a) Simulated data, genome-wide distribution of CMH $-\log(p\text{-values})$.

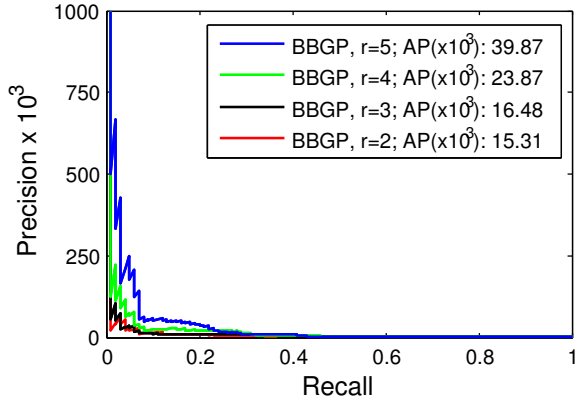


(b) Simulated data, genome-wide distribution of BBGP $\ln(\text{Bayes factors})$.

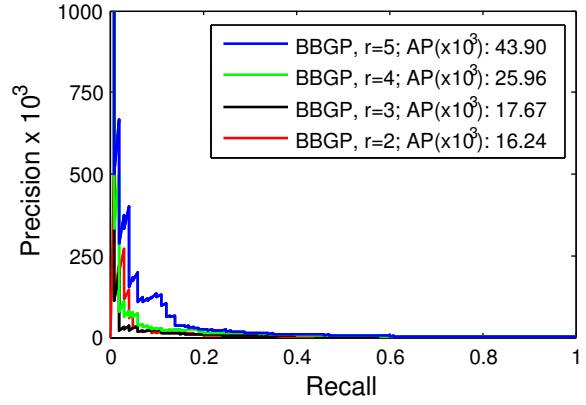
Figure 8: *Manhattan plots of genome-wide test statistic values on simulated data with 5 replicates.* (a) $-\log(p\text{-values})$ for the CMH test B-E comparison. (b) $\ln(\text{Bayes factors})$ for the BBGP using 6 time points. Only autosomal regions were simulated and low recombining regions ($< 1cM/Mb$) were excluded. The 100 truly selected SNPs ($s=0.1$) are indicated in red. As the consequence of linkage structure, we observe extended peaks in the vicinity of selected SNPs. However, there are still some truly selected SNPs that do not show clear pattern of frequency increase. A possible explanation for that can be that the time course, i.e. 60 generations, is not long enough for them to rise significantly in frequency. They can also interfere with each other and non-selected SNPs.



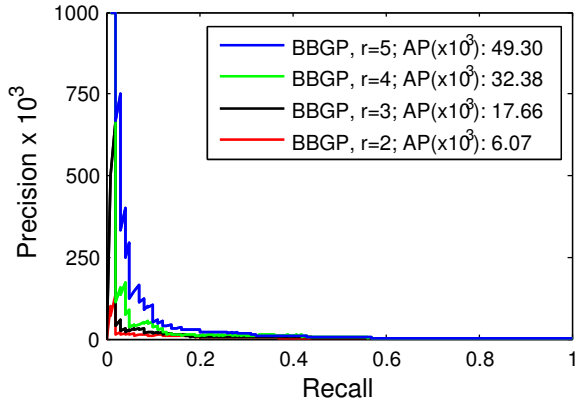
(a) CMH



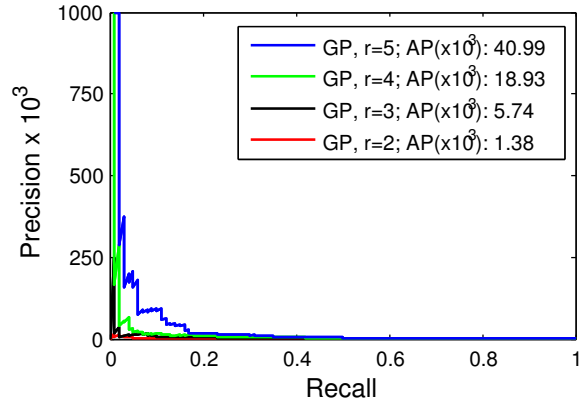
(b) BBGP (3 time points)



(c) BBGP (6 time points)



(d) BBGP (9 time points)



(e) GP (6 time points)

Figure 9: *Full precision-recall curves for the CMH and BBGP methods for Fig. 5. The precision is plotted as the function of recall for every possible cutoff value in the ranked sequence of candidate SNPs. The graph in Fig. 5 shows the average precisions for all replicate, time-point combinations.*

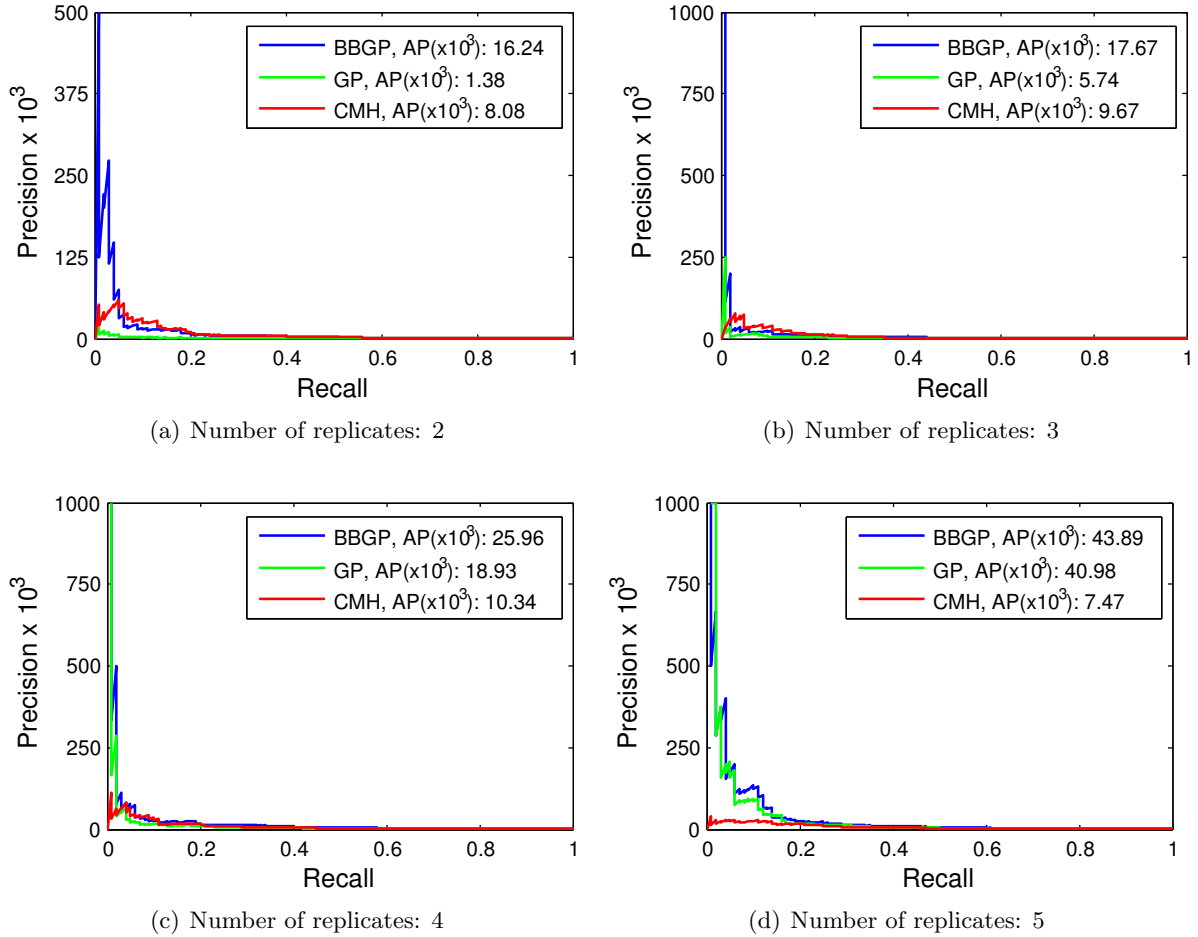


Figure 10: Precision recall curves comparing CMH method to the standard GP and BBGP methods using different number of replicates and 6 time points on whole-genome simulation. Incorporation of the beta-binomial posterior variances into the GP model provides the most benefit when the number of replicates are small. The more replication is performed during the experiments, the better performance can be expected from the GP-based methods. The CMH test, however, does not benefit from more replicates in the same way.

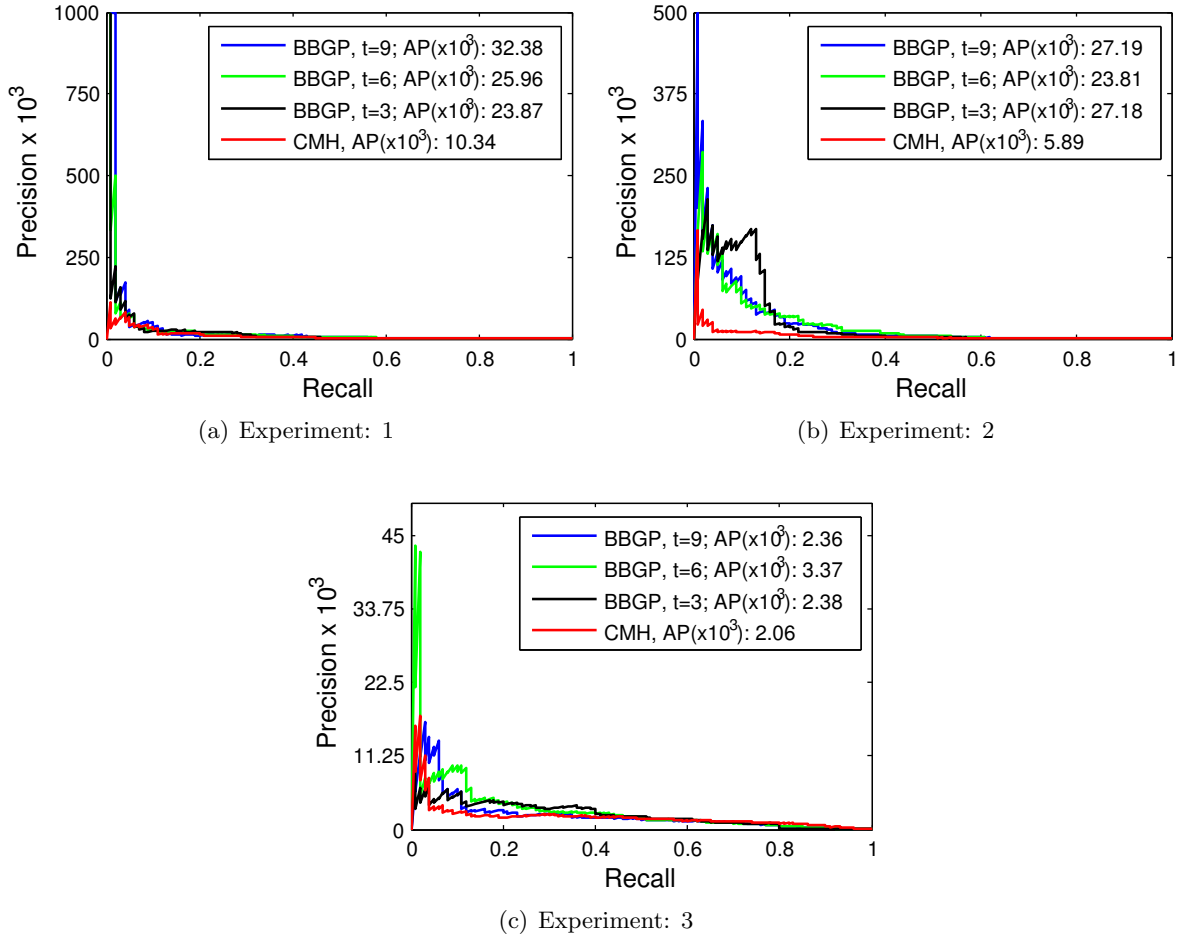


Figure 11: Precision recall curves comparing CMH to BBGP for 3 independent whole-genome experiments. The performance can vary noticeably between experiments (e.g., factor of 10 difference in AP between Experiment 1 and 3). Nevertheless, the BBGP based test consistently outperforms the CMH test.

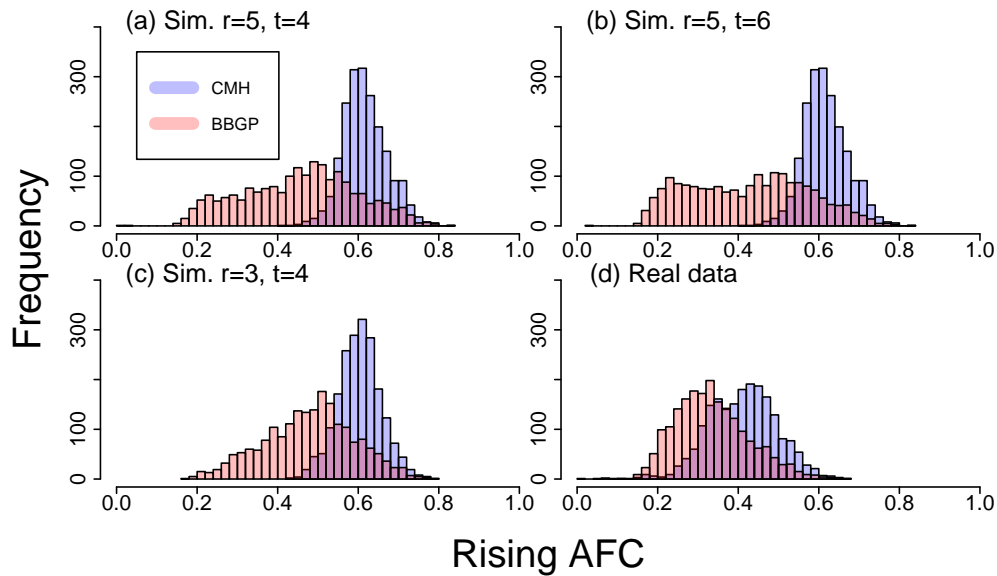


Figure 12: *Distribution of the average allele frequency change (AFC) of the rising allele for the top 2000 candidates in the whole-genome experiment.* AFC was calculated for each SNPs based on the average difference between the base and end populations across replicates. (a-b) AFC of the top 2000 candidates of the simulated data with 5 replicates, BBGP is performed on 4 (a) and 6 (b) time points, respectively. (c) AFC of the top 2000 candidates of the simulated data with 3 replicates, BBGP is performed on 4 time points. (d) AFC of the top 2000 candidates of the real data. We observed a significant location shift between the AFC distributions among the top 2000 candidate SNPs of the CMH and the BBGP (Mann-Whitney U, p -value $< 2.2e-16$ for all panels). The location shift indicates that the CMH test mostly captures radical AFC while the GP-based methods are also sensitive to consistent signals coming from intermediate time points.

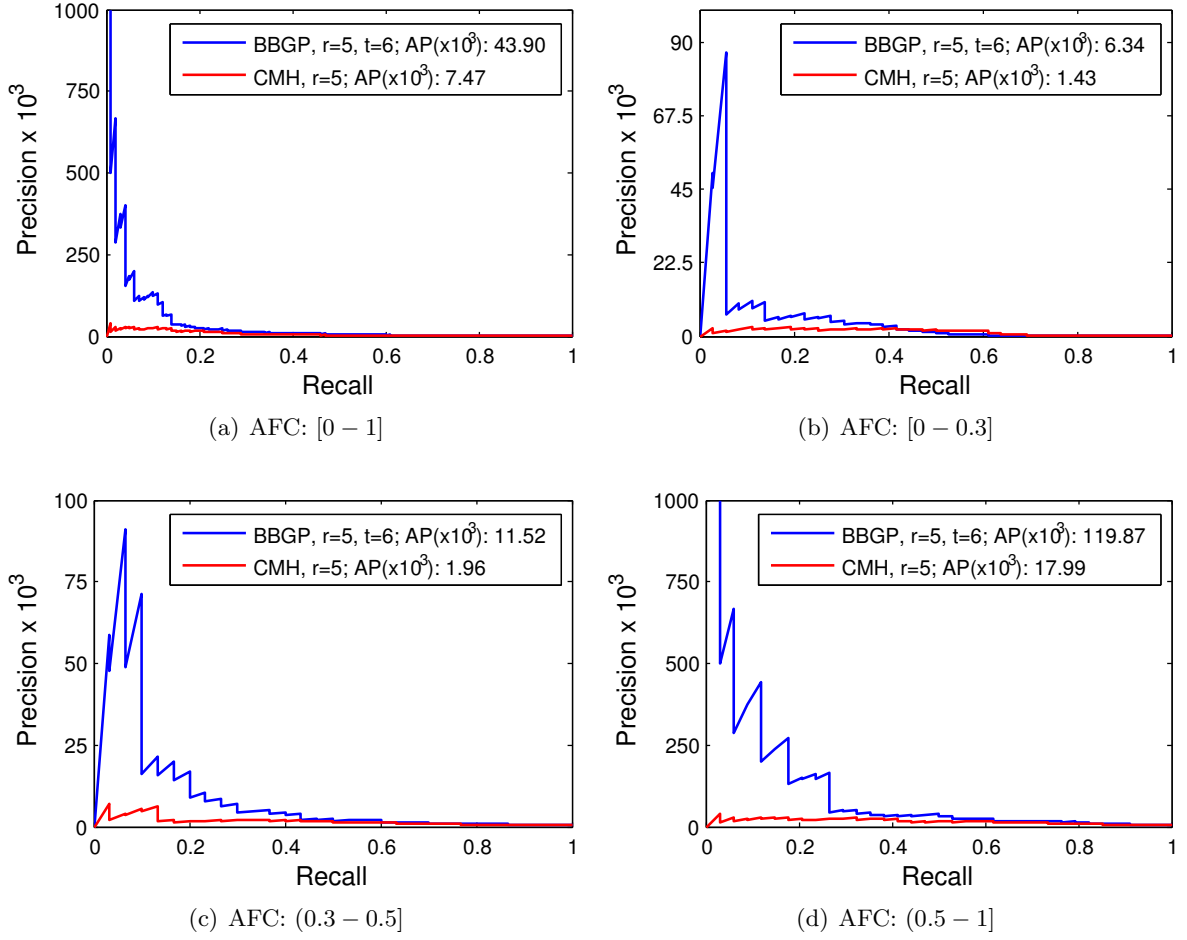


Figure 13: *Precision recall curves for different AFC classes in the whole-genome simulation.* The performance in terms of precision and recall is shown for the CMH and the BBGP in classes of SNPs with different allele frequency change. The AFC is measured between the base and end generations (60) and averaged over 5 replicates. 6 time points were used for the BBGP. Panel (a) shows the overall performance. In panels (b)-(d), the AFC classes contain the following number of selected SNPs: 36 in class [0-0.3], 30 in class (0.3-0.5], 34 in class (0.5-1.0].

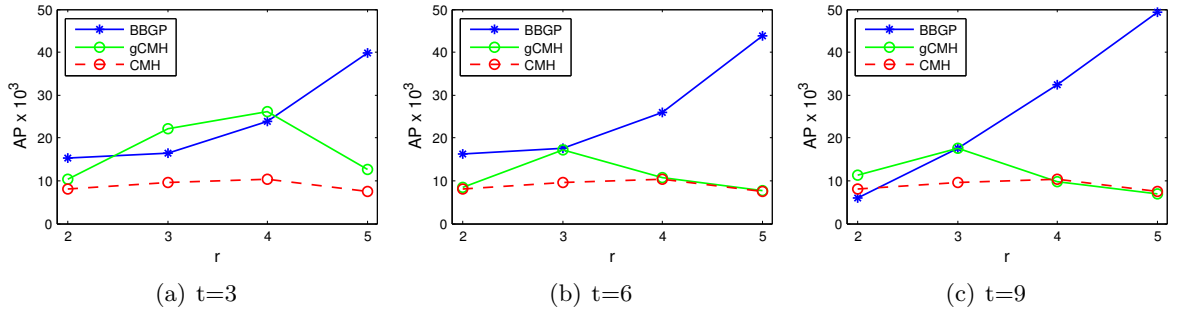


Figure 14: *Average precision of the different methods with different number of time points and replicates in the whole-genome simulation.* Average precisions for the BBGP and the CMH test are same as on Fig. 5. Precisions of the generalised CMH test (gCMH) are added in green for every possible time-replicate combinations to the figures.

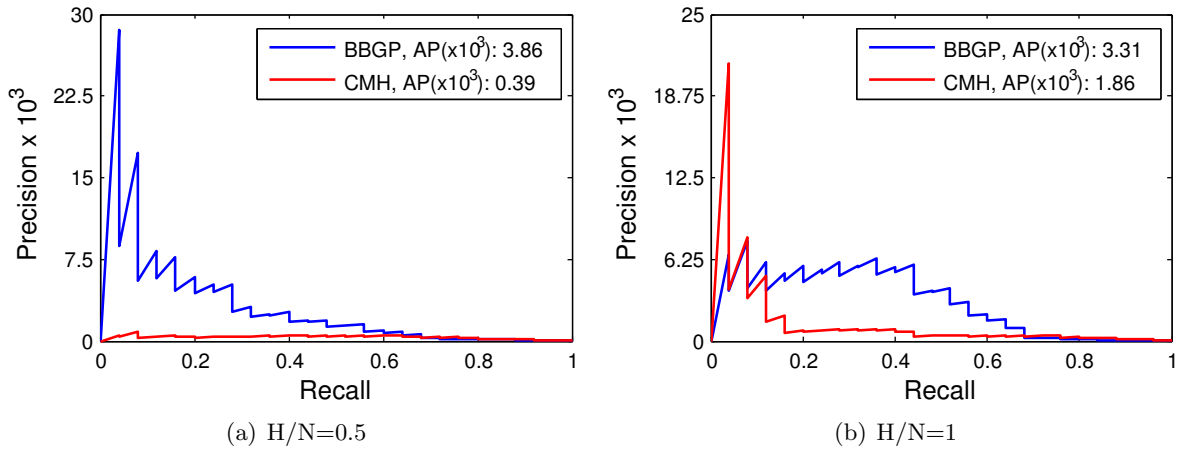


Figure 15: Precision recall curves comparing CMH to BBGP for different H/N ratios for $N=200$ in the single-chromosome-arm simulation.

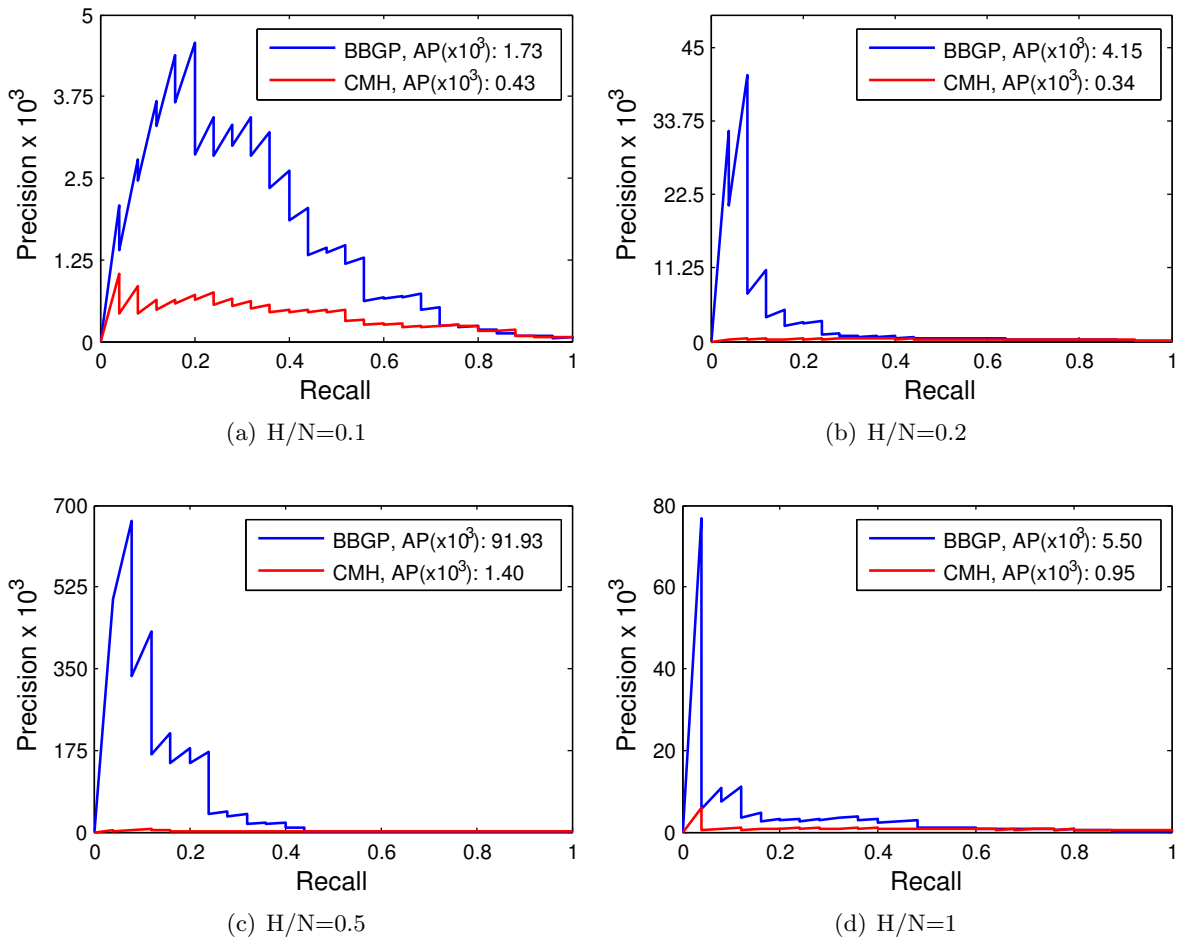


Figure 16: Precision recall curves comparing CMH to BBGP for different H/N ratios for $N=1000$ in the single-chromosome-arm simulation.

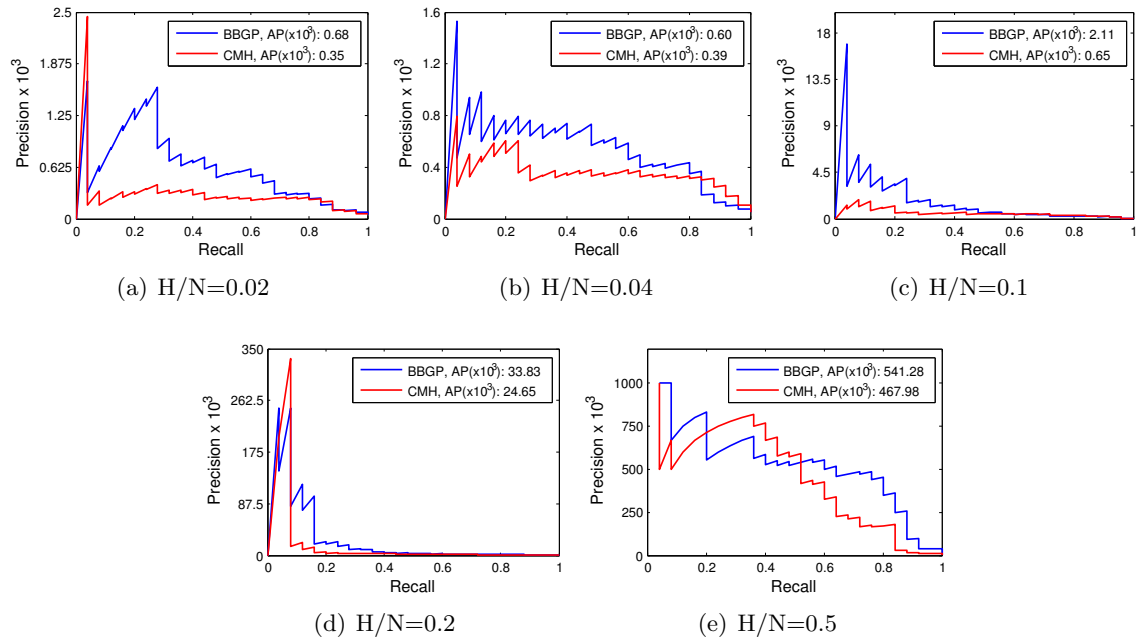


Figure 17: Precision recall curves comparing CMH to BBGP for different H/N ratios for $N=5000$ in the single-chromosome-arm simulation.

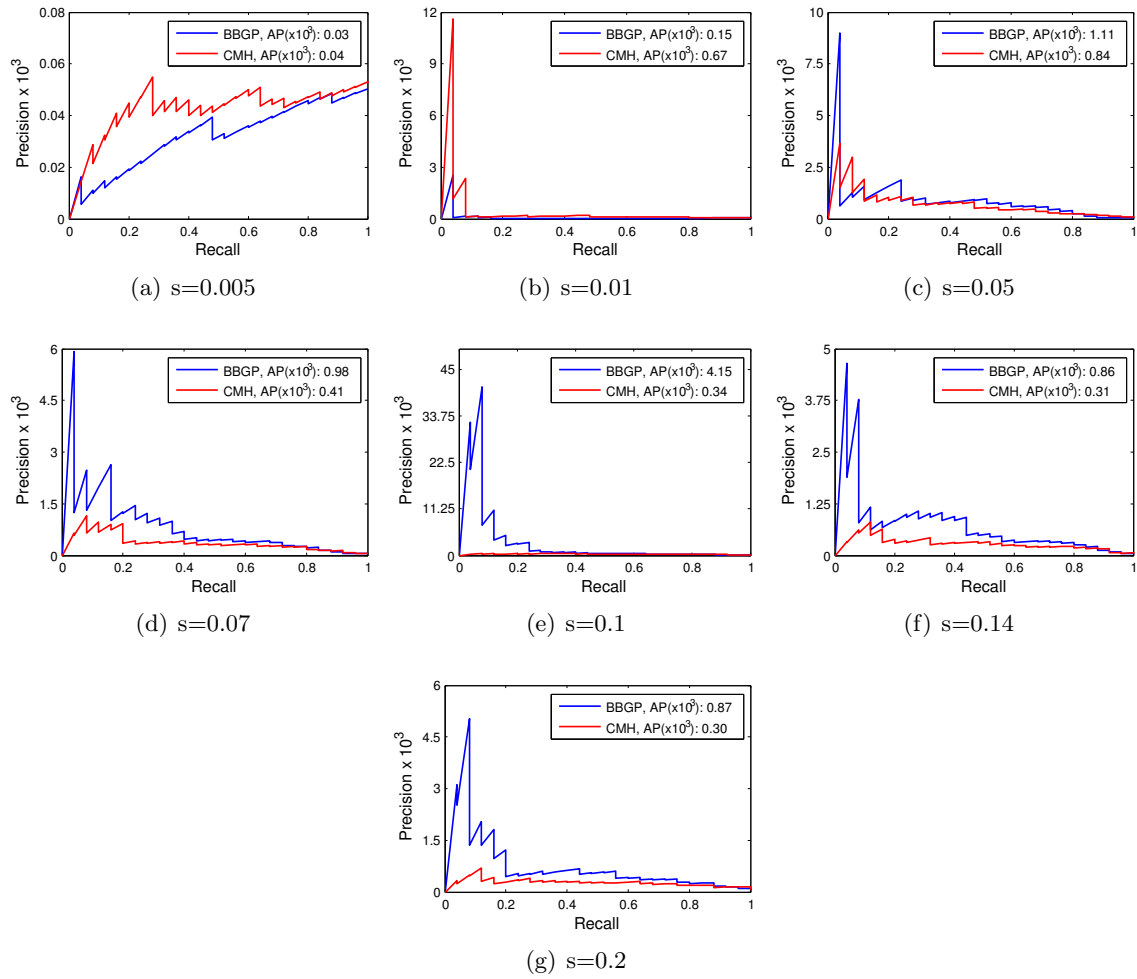


Figure 18: Precision recall curves comparing CMH to BBGP for different selection coefficients (s) in the single-chromosome-arm simulation.

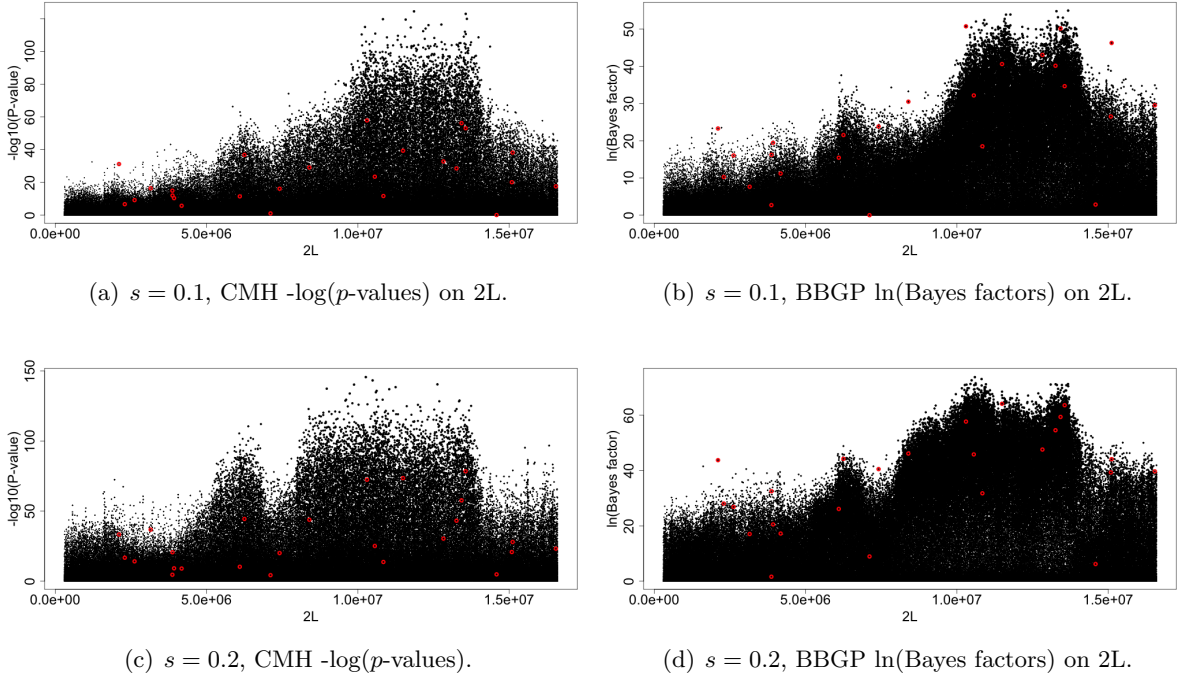


Figure 19: *Manhattan plots of test statistic values for simulations with a single chromosome arm.* (a,c) $-\log(p\text{-values})$ for the CMH test B-G60 comparison for 5 replicates. (b,d) $\ln(\text{Bayes factors})$ for the BBGP using 6 time points and 5 replicates. Truly selected SNPs ($s=0.1$ (a-b); $s=0.2$ (c-d)) are indicated in red.

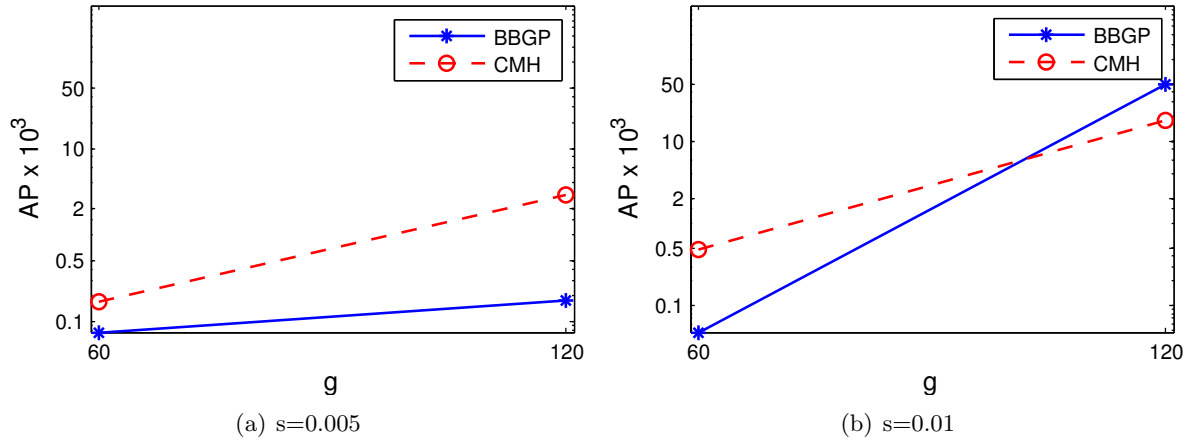


Figure 20: *Average precision with weak selection and large population size ($N = 5000$, $H = 2500$).* Log scale was used on y axis. The performance of the methods is shown when large populations evolved under weak selection. Under the basic parameter setup (Fig. 6(b)) the CMH outperforms the BBGP for weak selection strength of $s = 0.005$ and 0.01 . We observe the same behaviour even with larger population size ($N = 5000$, $H = 2500$) when the performance is evaluated using data up to generation 60. However, if we let the populations evolve further until generation 120, the BBGP gain a large performance improvement over the CMH test for $s = 0.01$. For weaker selection, we suppose that the BBGP would need even more time to outperform the CMH test.

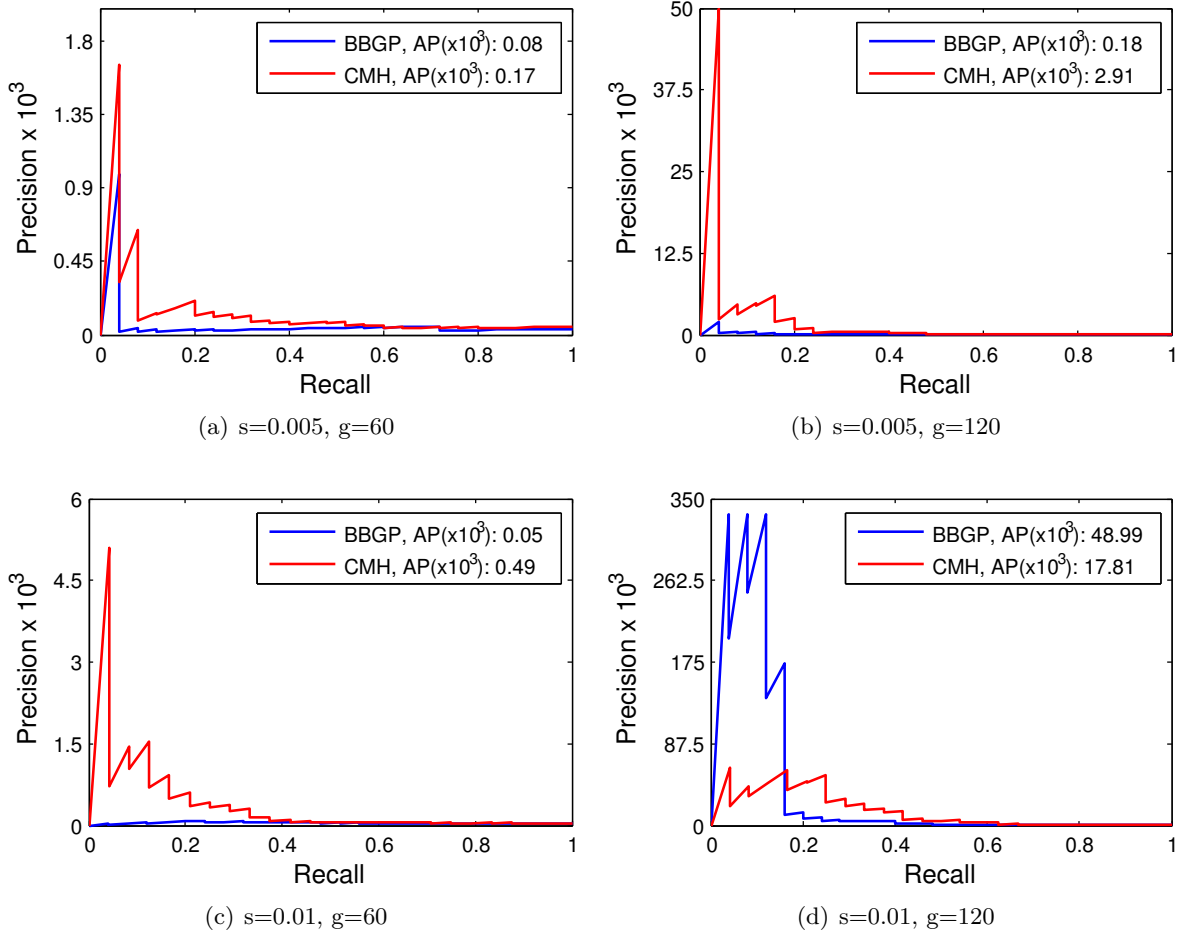


Figure 21: Precision recall curves comparing CMH to BBGP with weak selection for different time durations in the single-chromosome-arm simulation. 6 time points were used in the BBGP: $\{0, 12, 24, 36, 48, 60\}$ and $\{0, 24, 48, 72, 96, 120\}$ for 60-generation and 120-generation experiments, respectively.

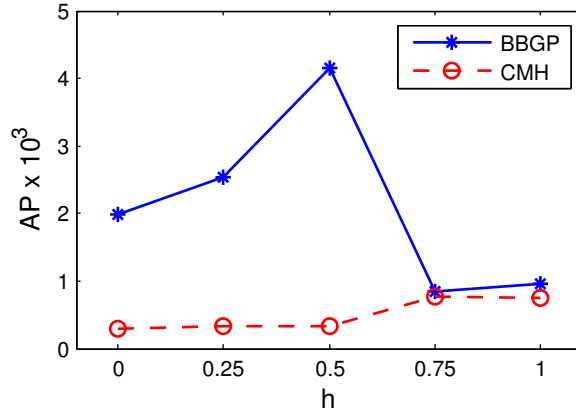


Figure 22: Average precision for different levels of dominance (h) in the single-chromosome-arm simulation.

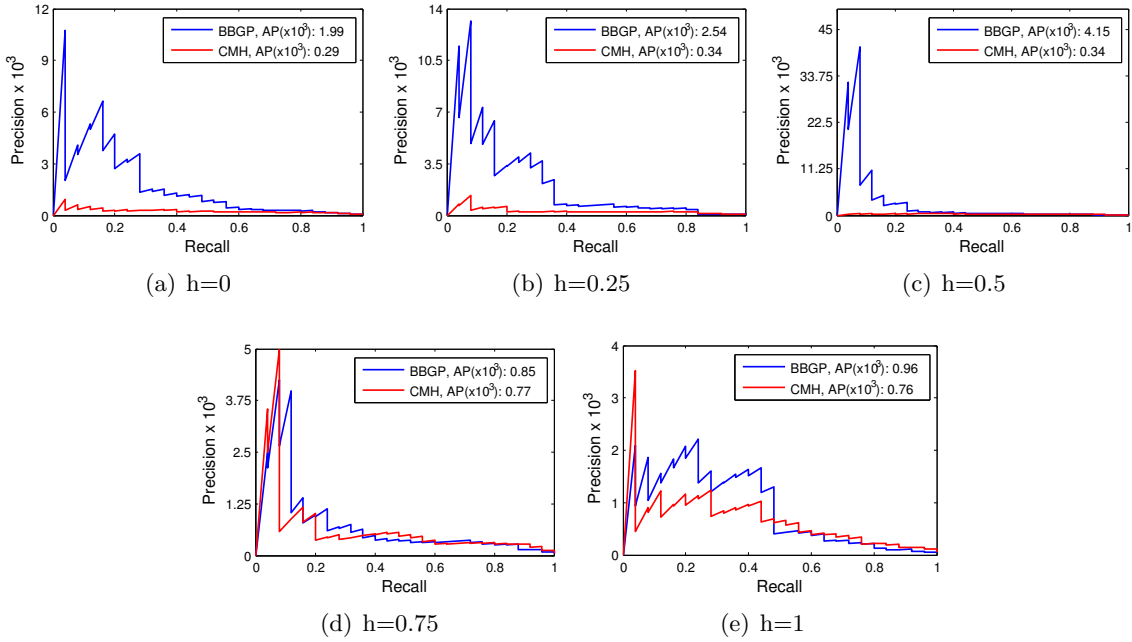


Figure 23: Precision recall curves comparing CMH to BBGP for different dominance levels (h) in the single-chromosome-arm simulation.

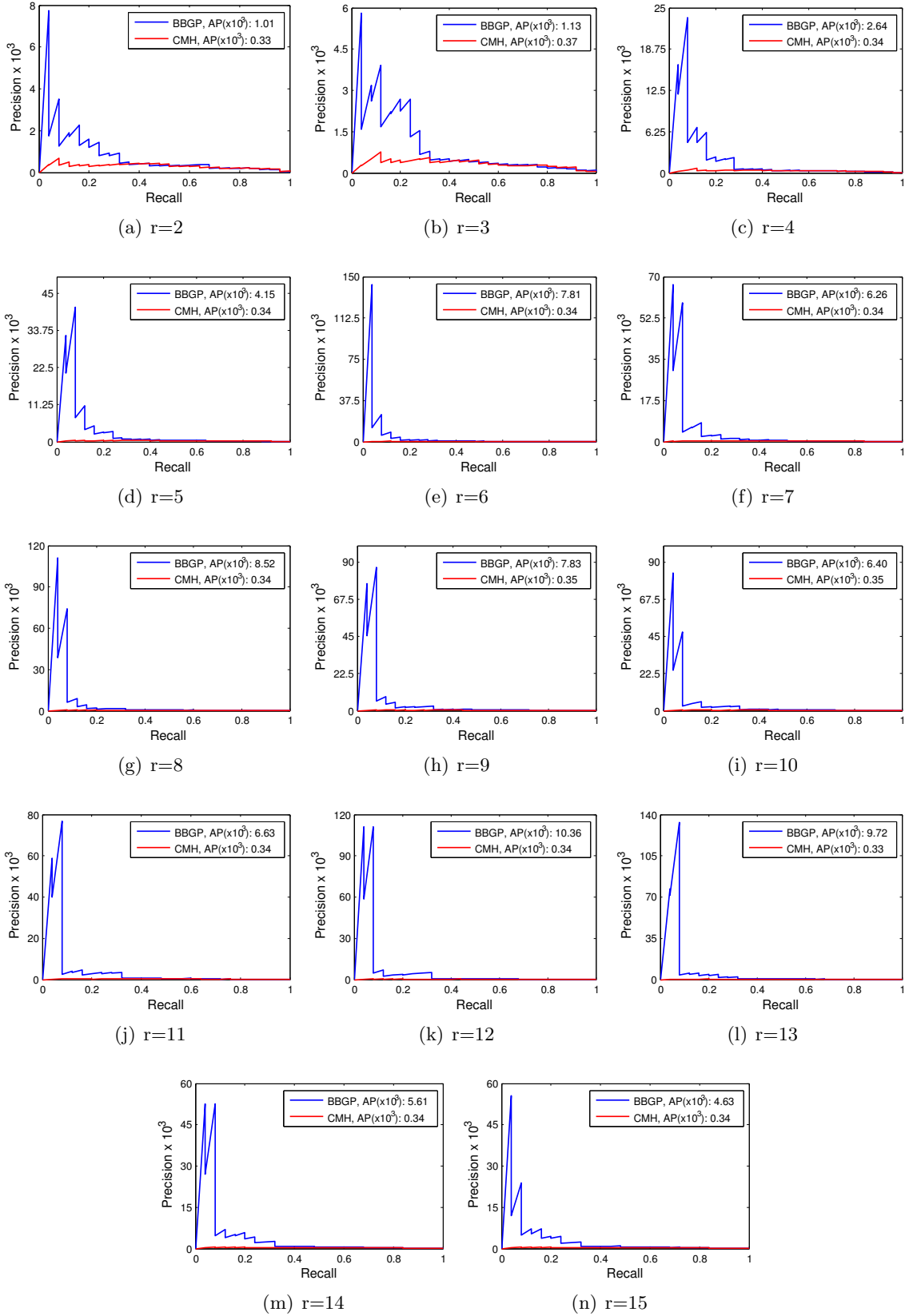


Figure 24: Precision recall curves comparing CMH to BBGP for different number of replicates (r) in the single-chromosome-arm simulation.

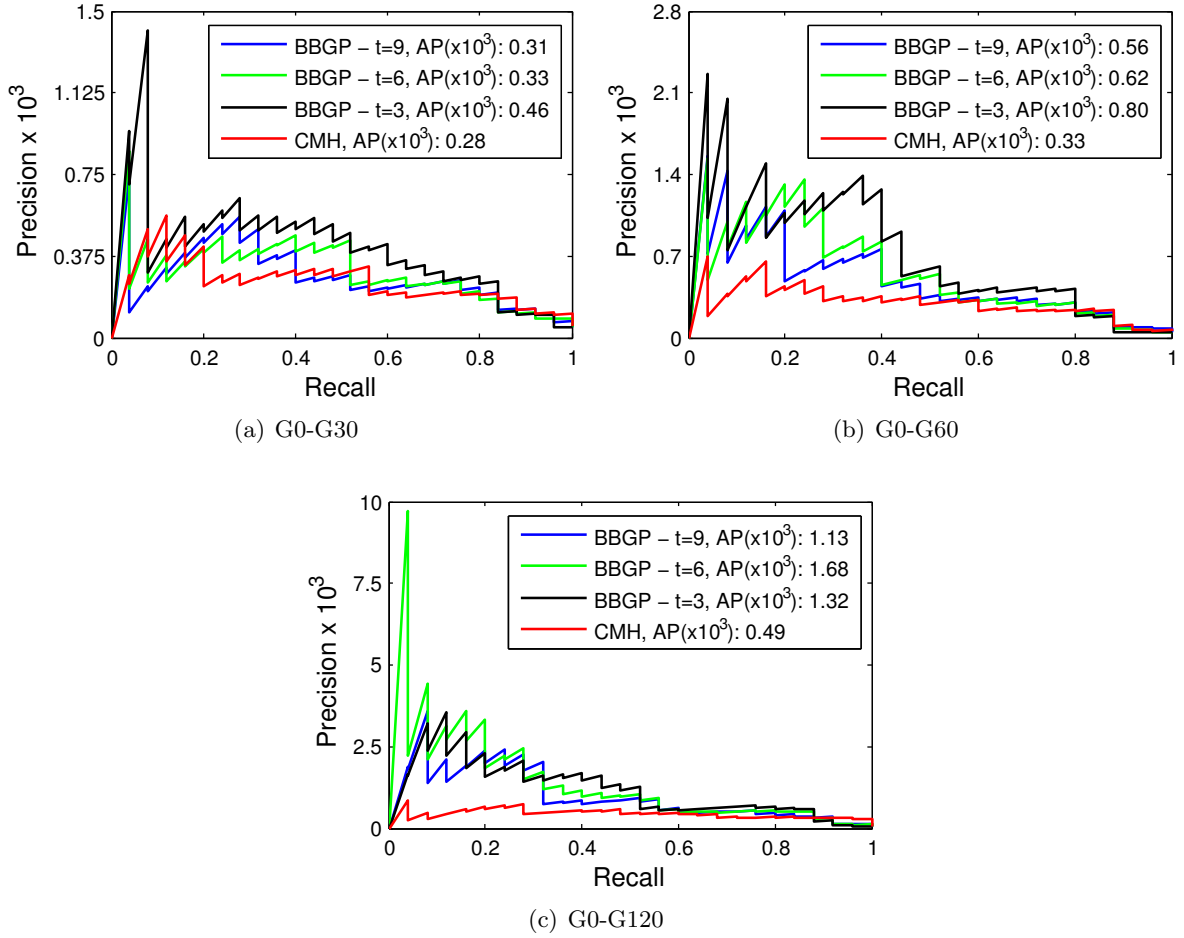


Figure 25: Precision recall curves comparing CMH to BBGP using different number of time points combined with different experiment lengths (single-chromosome-arm simulation). In order to investigate the effects of the time spacing as well as the duration of the experiment, the following sampling schemes were applied on the time points:

G0-G30: $\{0, 18, 30\}$, $\{0, 6, 12, 18, 24, 30\}$, $\{0, 4, 6, 10, 14, 18, 22, 26, 30\}$;

G0-G60: $\{0, 36, 60\}$, $\{0, 12, 24, 36, 48, 60\}$, $\{0, 8, 12, 20, 28, 36, 44, 52, 60\}$;

G0-G120: $\{0, 72, 120\}$, $\{0, 24, 48, 72, 96, 120\}$, $\{0, 16, 24, 40, 56, 72, 88, 104, 120\}$.

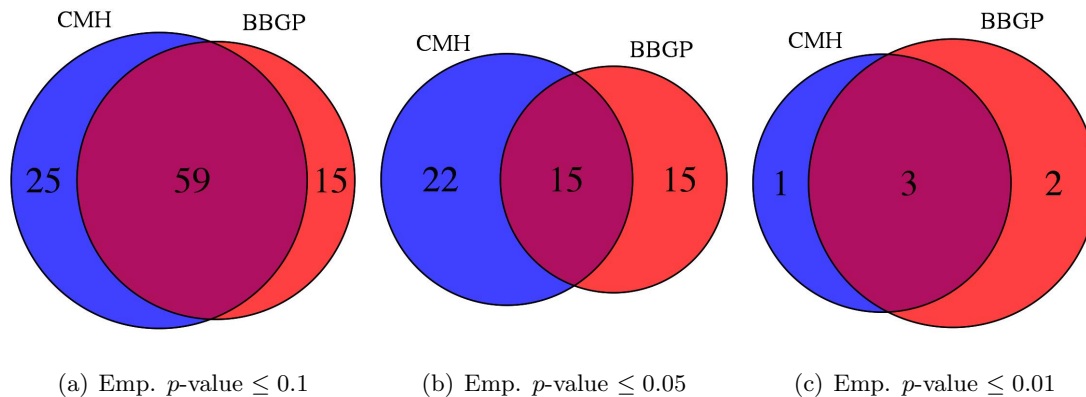


Figure 26: *Venn diagram of significantly enriched GO categories.* Empirical p -values (Emp. p -val.) for the MWU tests are calculated for each category based on sampling random SNPs (1000 times) but keeping their chromosomal order. Overlaps between CMH and BBGP tests are shown for different significance levels.

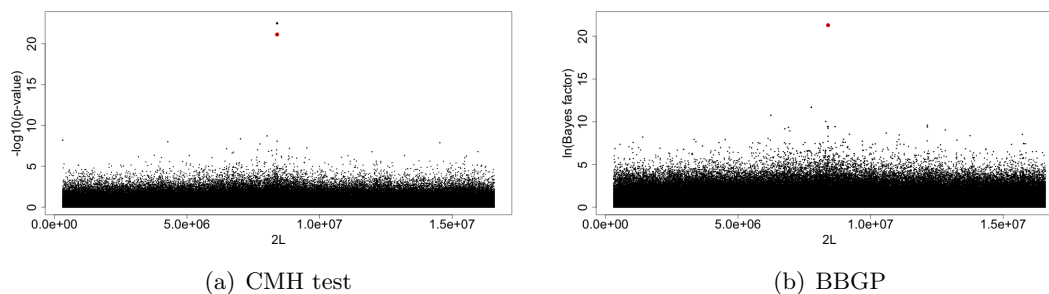


Figure 27: *Manhattan plots on simulated data using only a single selected SNP ($s = 0.1$) on the whole chromosome arm.* Simulation was performed as described in Section 2.7 on a single chromosome arm of $2L$ ($\sim 16Mb$) using the basic parameter setup. The only difference is the number of SNPs assigned to be selected. Here we used a single selected SNP on the middle of the chromosome (highlighted in red) to see how much influence does the interference between selected SNPs play in shaping the dynamics of allele frequency trajectories. We see striking evidence that high number of false positives are due to interactions between linked selected sites.

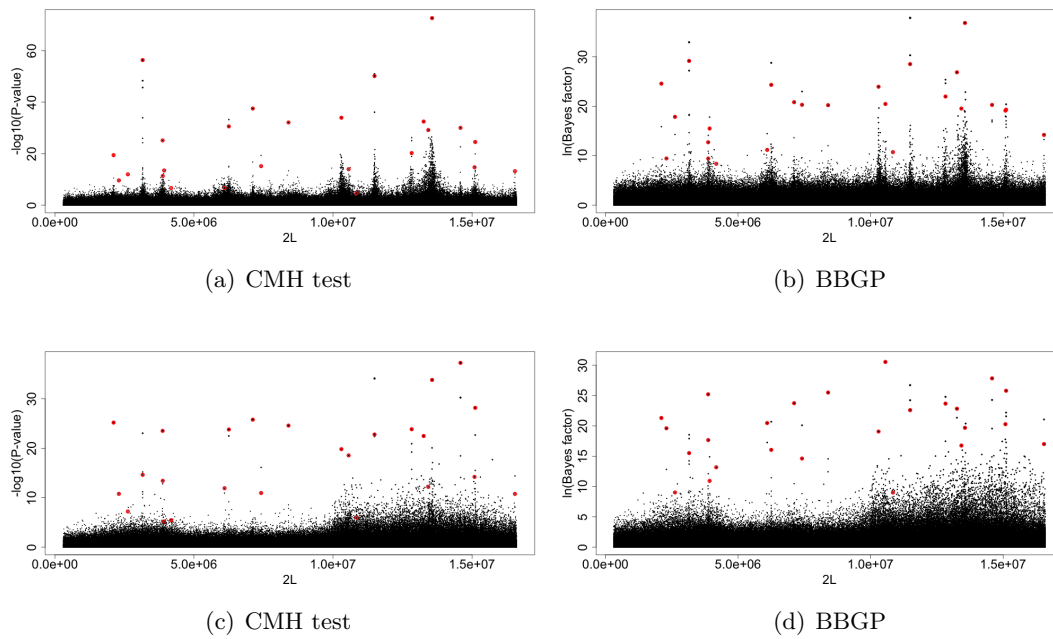


Figure 28: *Manhattan plots with high recombination rate (a-b) and large population size (c-d).* Top row (a-b): Simulation, as described in Section 2.7, was carried out by setting high recombination rate uniformly across $2L$. Bottom row (c-d): Simulation with normal level of recombination but using large populations size of $N = 5000, H = 2500$. Selected SNPs are indicated in red. Linkage is broken up when large population size is used for simulations (c-d) and the dynamics of allele trajectories become more similar to the ones that are simulated with high recombination rate (a-b). For experimental design, however, recombination rates cannot be easily modified but similar effect can be attained by propagating larger populations.

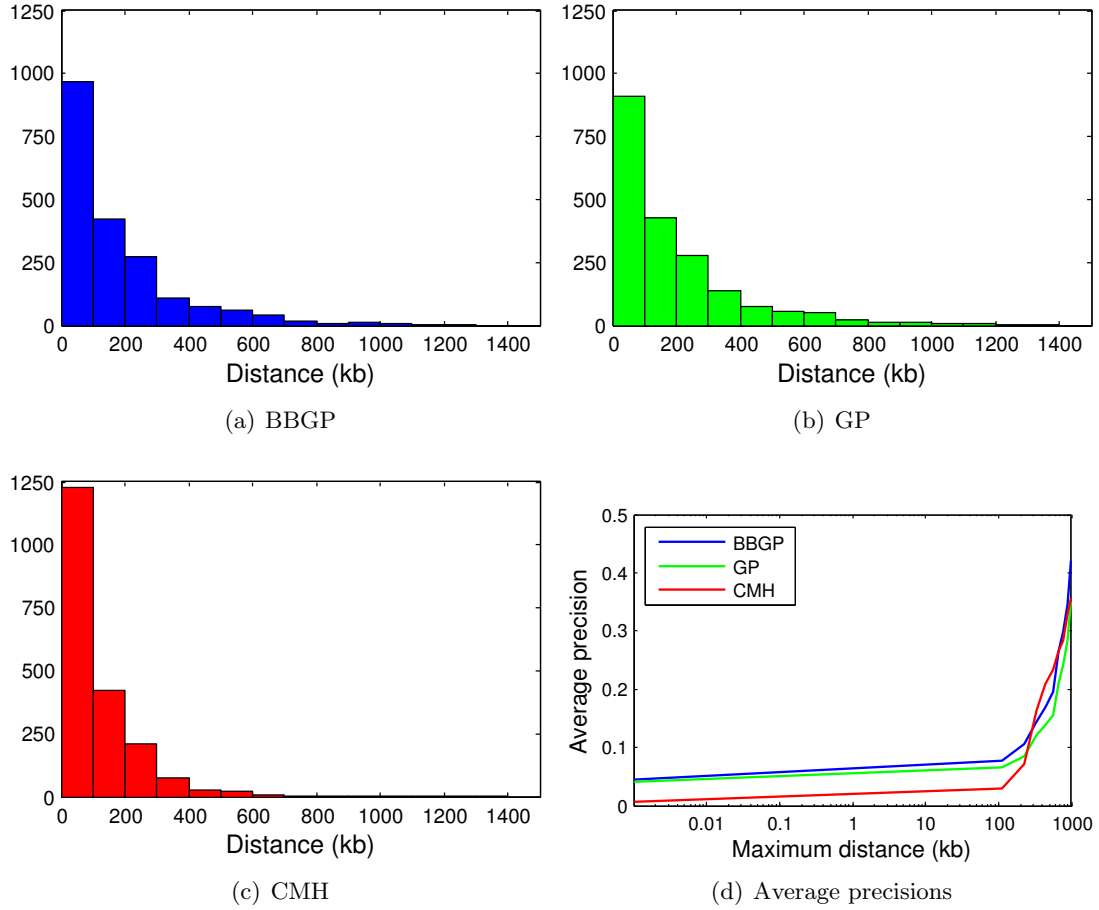


Figure 29: *Distribution of the distances (kb) to the nearest selected SNPs for the top 2000 candidate SNPs (a-c) and average precisions when potential hitchhikers are excluded (d). The lines in panel (d) show the performances of the methods when the potential hitchhikers, i.e. non-selected SNPs closer than the given distance from a selected SNP, are excluded prior to the calculation of the average precisions. Log-scale was used on x -axis, which shows the maximum distance (kb) of the excluded potential hitchhikers to the nearest selected SNPs. The plots were obtained from whole-genome simulation data with 5 replicates and 6 time points.*